NASA CR—145011

TECHNIQUES FOR COMPUTING REGIONAL RADIANT EMITTANCES OF THE EARTH-ATMOSPHERE SYSTEM FROM OBSERVATIONS BY WIDE-ANGLE SATELLITE RADIOMETERS

By José F. Pina and
Frederick B. House

EARTH ENERGY EXPERIMENT (E^3) PROJECT

NASA CONTRACT NAS 1-11871

drexel university

DEPARTMENT OF PHYSICS
AND ATMOSPHERIC SCIENCE

NASA CR - 145011

TECHNIQUES FOR COMPUTING REGIONAL RADIANT EMITTANCES OF THE EARTH-ATMOSPHERE SYSTEM FROM OBSERVATIONS BY WIDE-ANGLE SATELLITE RADIOMETERS

By José F. Pina and
Frederick B. House

Final Report
Phase III

Prepared under Contract No. NAS1-11871 by
Department of Physics and Atmospheric Science
Drexel University
Philadelphia, Pennsylvania 19104

for

NATIONAL AERONAUTICS AND SPACE ADMINISTRATION

August, 1975

PREFACE

The present report contains results of an investigation of critical problems related to satellite systems for long-term earth energy budget (EEB) observations, performed under Langley Research Center Contract No. NAS1-11871 for the National Aeronautics and Space Administration.

This research study, performed by Drexel University, is one part of a much larger effort by several institutions, including Colorado State University, The University of Wisconsin, Virginia Polytechnic Institute and State University, Link Temco Vought as well as cognizant personnel at NASA Langley Research Center. This team is studying satellite systems for performing long-term EEB measurements over geographical regions, hemispheres, and the entire earth for periods of 10 to 30 years. A major portion of the total effort is responsive to the AAFE proposal, and the proposed LZEEBE system (reference 1) which employs three balloon radiometers.

The decision was made to expand the scope of the total effort beyond that envisioned in the AFFE proposal. This boradened scope includes Phase A type of efforts concerning other concepts of performing EEB observations besides the balloon system. For example, systems employing spinning plate radiometers and/or scanning radiometers could be developed for long-term space application. Regardless of the geometric characteristic of the observational system, the problems of data analysis and interpretation are similar for all wide-angle systems with only an adjustment required for viewing geometry.

The current investigation was performed during the twelve month period 1 January 1974 through 31 December 1974. This period is denoted as Phase III in subject contract. The express purpose of the investigation is outlined in the following objectives, contained in the statement of work.

1. Accuracy assessment of Sampling Bias by Candidate Satellite Systems for EEB Observations
2. Development of Procedures for Analysis and Interpretation of EEB Observations by Wide-field, Broad-band Detectors
3. Accuracy Assessment of Procedures for Analysis and Interpretation of EEB Observations
4. Specification of Spectral Absorbing Characteristics of Broad-band Detectors and Calibration Requirements for Accurate Observation of the EEB
5. Variance Spectrum Analysis of EEB Observations from ESSA VII Satellite
6. Professional Support and Advisory Effort as Co-Principal Investigator of LZEEBE

This report is the final report for the phase III effort under NASA Contract No. NAS1-11871. Other reports that are related to the overall effort are: "An Investigation of ESSA VII Radiation Data for Use in Long-term Earth Energy Experiments," published as NASA CR-132623; "Our Contaminated Atmosphere - The Danger of Climate Change," published as NASA CR-132625 and "Steady-state Solution to the Conduction Problem of a Spherical Balloon Radiometers," published as NASA CR-132624.

Gratitude is extended to several NASA/LaRC personnel for their encouragement, interest, stimulating discussions and suggestions provided during the present investigation. Among these scientific personnel are included: Messrs. George Sweet (technical monitor), Charles Woerner, Jack Cooper, Dr. Louis Smith and other members of the LaRC team.

Frederick B. House, Project Director
Associate Professor of Physics and
Atmospheric Science

CONTENTS

LIST OF FIGURES

LIST OF TABLES

LIST OF SYMBOLS AND ACRONYMS

Symbol	Definition	First used in Equation	First used on Page
Q	Net Flux*, W/m^2	1-1	1-1
H_s	Solar irradiance, W/m^2	1-1	1-1
W_r	Radiant reflectance, W/m^2	1-1	1-1
W_e	Radiant emittance, W/m^2	1-1	1-1
A	Instantaneous albedo, dimensionless	1-2	1-1
P	Radiant power intercepted by a satellite, W	2-1	2-2
F	Shape, or configuration factor, dimensionless	2-1	2-2
P_α	Power absorbed by a satellite, W	2-2	2-2
α	Absorptance of the satellite, W	2-2	2-2
α	Nadir angle	2-13	2-5
α_λ	Spectral absorptivity, dimensionless	2-3	2-3
ϵ_λ	Spectral emissivity, dimensionless	2-3	2-3
λ	Longitude, degrees	2-6	2-3
ϕ	Latitude, degrees	2-6	2-3
θ	Zenith angle	2-6	2-3
ψ	Azimuthal angle	2-6	2-3
t	Time, sec	2-6	2-3
N	Radiance, $W/(m^2\text{-sr})$	2-6	2-3
N^z	Radiance in the zenith direction, $W/(m2\text{-sr})$	2-7	2-4
N^{iso}	Isotropic radiance, $W/(m^2\text{-sr})$	2-12	2-5
f	Limb darkening function	2-7	2-4
I	Value of integral	2-10	2-4

* The quantities and names used throughout this report are based on those selected by Craig (reference 2).

LIST OF SYMBOLS AND ACRONYMS (Continued)

Symbol	Definition	First used in Equation	Page
E-A	Earth-atmosphere system		
R	Radius of the E-A system, m	2-15	2-5
H	Height of satellite, m	2-15	2-5
ΔA	Area element observed, m^2	Fig. 2-1	2-6
d	Distance from ΔA to the satellite, m	2-15	2-5
d_m	Distance from satellite to perimeter of FOV	Fig. 2-1	2-6
SSP	Satellite subpoint	Fig. 2-1	2-6
γ	Angle between SSP and ΔA, measured at the earth's center	Fig. 2-1	2-6
γ_m	Maximum value γ attains	Fig. 2-1	2-6
α_m	Maximum value of nadir angle	Fig. 2-1	2-6
ζ	Solar zenith angle at ΔA	Fig. 2-1	2-6
θ_m	Maximum value of the satellite's zenith angle θ	Fig. 2-1	2-6
ρ	Distance between SSP and ΔA in the flat E-A system, m	Fig. 2-1	2-6
ρ'	Distance between SSP and ΔA in the flat E-A system, degrees	Fig. 2-1	2-6
ρ_m	Maximum value ρ can attain	Fig. 2-1	2-6
ρ_s	Bidirectional reflectance	2-20	2-8
S	Solar constant; $S=1353\pm21$ W/m^2	2-16	2-7
L	Ratio of $\bar{d}^2$ to d^2	2-16	2-7
$\bar{d}$	Mean sun-to-earth distance		
d	Instantaneous sun-to-earth distance		
N_r	Radiance of reflected SWR, W/(m^2-sr)	2-19	2-8
r	Directional reflectance, dimensionless	2-20	2-8
P_{in}	Radiant input power to radiometer, W	2-26	2-11

Symbol	Definition	First used in Equation	Page
P_{out}	Radiant output power from radiometer, W	2-28	2-11
σ	Stefan-Boltzmann constant, σ=5.6697x10^{-8} W/(m^{2}-^{o}K^{4})	2-28	2-11
F_{sp}	Shape factor for a sphere	2-36	2-13
F_{pl}	Shape factor for a plate	2-37	2-13
F_{sp}^{iso}	Isotropic shape factor for a sphere	2-40	2-13
F_{pl}^{iso}	Isotropic shape factor for a plate	2-41	2-13
R_k	kh region	3-6	3-6
ΔA_{ijk}	ith area element in the kth region within the FOV of the jth observation	3-8	3-8
ΔP_{ijk}	Power increment contributed by ΔA_{ijk}	3-8	3-8
N_{ijk}	Radiance of ΔA_{ijk} in the direction of the radiometer	3-8	3-8
A_s	Characteristic area of radiometer = πa^2 for sphere and plate (a = radius)	3-8	3-8
d_{ijk}	Distance from ΔA_{ijk} to radiometer	3-8	3-8
α_{ijk}	Nadir angle of ΔA_{ijk}	3-9	3-8
F_{ijk}	Shape factor contributed by ΔA_{ijk}	3-18	3-14
F_{jk}	Shape factor of segment of kth region within the FOV of jth observation	3-24	3-15
P_j	Total power intercepted by the radiometer in the jth observation	3-26	3-16
F	n by n configuration factor matrix	3-30	3-16
$\{W_e\}$	Radiant emittance n column matrix	3-30	3-16
$\{P\}$	Radiant power n column matrix	3-30	3-16
F^{-1}	Inverse of matrix F	4-3	4-1
δP	Uncertainty in P	4-4	4-2
δW_e	Uncertainty in W_e	4-5	4-2
W_e'	W_e plus its uncertainty	4-4	4-2

Symbol	Definition	First used in Equation	Page
$\tilde{F}^{-1}$	Inverse of stabilized configuration factor matrix	4-9	4-3
$\delta\tilde{W}_e$	New uncertainty in W_e by multiplying $\tilde{F}^{-1}$ by δP	4-9	4-3
Δ_{long}	Longitude of ΔA minus longitude of SSP	4-19	4-10
Δ_{lat}	Latitude of ΔA minus latitude of SSP	4-19	4-10
$\vert\lambda_{max}\vert$	Largest modulus eigenvalue of F	4-49	4-27
$\vert\lambda_{min}\vert$	Smallest modulus eigenvalue of F	4-49	4-27
C_1	Condition number of F	4-49	4-27
C_2	Condition number of F	4-45	4-26
rel $\{W_e\}$	Relative error of W_e	4-45	4-26
rel $\{P\}$	Relative error of P	4-45	4-26
$\Vert F\Vert_1$	Column norm of F	4-51	4-27
$\Vert F\Vert_\infty$	Row norm of F	4-52	4-27
Tr F	Trace of F		
$\vert F\vert$	Determinant of F		
λ_i	ith eigenvalue of F		
SS_j	Sum of the elements in the jth column of F for the sphere	4-53	4-41
SP_j	Sum of the elements in the jth column of F for the plate	4-53'	4-41
F^S_{jj}	Diagonal element of F for the sphere	4-55	4-41
F^P_{jj}	Diagonal element of F for the plate	4-55'	4-41
W_{ei}	Plain, or unweighted average of W_e	4-58	4-44
W^A_{ei}	Weighted average of W_e (weight is the area A)	4-59	4-44

LIST OF SYMBOLS AND ACRONYMS (Continued)

Symbol	Definition	First used in Equation	Page
W^F_{ei}	Weighted average of W_e (weight is the configuration factor F)		
We_{ij}	The jth determination of the value of W_e for the ith region	4-58	4-44
A_{ij}	Total area seen of the ith region during the jth observation set	4-59	4-44
F_{ij}	Sum of all the configuration factors of the ith region which entered in the jth observation set.	4-60	4-44
r_{ijk}	Directional reflectance by ΔA_{ijk}	4-63	4-47
$r_k(o)$	Directional reflectance of the kth region for zero solar zenith angle	4-63	4-47
R_{ijk}	Reading from figure 5, reference 3	4-63	4-47
R'_{ijk}	Reading from figures B-3, B-4, or B-5 of reference 3	4-69	4-48
R''_{ijk}	Defined as R_{ijk} (ζ) cos (ζ)	4-86	4-51

Acronyms

EEB	Earth Energy Budget
AAFE	Advanced Application Flight Experiment
LZEEBE	Long-term Zonal Earth Energy Budget Experiment
GARP	Global Atmosphere Research Project

INTRODUCTION

The study of the total energy budget of the planet earth and its atmosphere is based on analysis of the exchange of radiant energy between the earth-atmosphere (E-A) system and space. Radiometers on earth-orbiting satellites can effectively measure this exchange of radiant energy at observation points in space external to the E-A system. The current effort is concerned with the analysis and interpretation of observations by wideangle, spherical and flat radiometers with regard to the general problem of the earth energy Budget (EEB); but in particular, it is concerned with the problem of determining the energy budget of regions smaller than the field of view (FOV) of these radiometers. Before considering specific reasons or motivations for conducting the present research effort, the background to the overall problem will be discussed.

Background

The energy budget at a specific time t for a given region of the E-A system's surface can be described by the following expression which shows the relationship of the net flux Q to the three fluxes H_s, W_r, and W_e.

$$Q = H_s - (W_r + W_e) \tag{1-1}$$

The meaning of the three fluxes is shown schematically in figure 1-1. The symbols Q, H_s, W_r, and W_e are defined in the List of Symbols in the front matter of this report. Introducing the concept of albedo $A = W_r/H_s$, which is also depicted in Figure 1-1, one can rewrite (1-1) as

$$Q = H_s (1 - A) - W_e \tag{1-2}$$

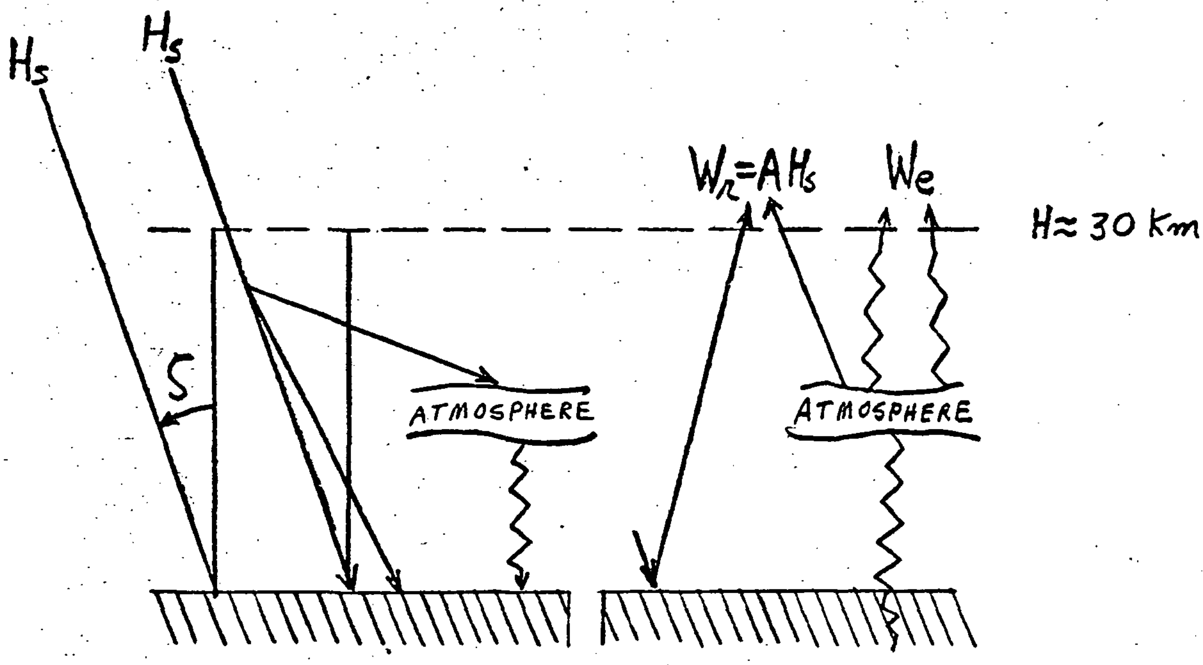

Figure 1-1. Radiant power balance on an earth surface element.

A time average of the net flux $\overline{Q}$ over any convenient time scale can be readily computed from the data available for any of the E-A system regions that has been under study.

The net flux Q defined by equation (1-1) can represent the time average conditions for a broad range of spatial dimensions. These can range from the dimensions of a GARP grid, about $5^{\circ} \times 5^{\circ}$ great circle arc, to the dimensions of the entire globe. Different observational satellite systems must be employed to perform the required measurements over this broad range of spatial dimensions. For example, a scanning radiometer would be needed to observe the components of net flux for a GARP grid. On the other hand, a wide-angle radiometer can best fulfill the sampling requirements for the entire globe. In terms of conventional meteorological dimensions a GARP grid maybe classed as a mesoscale feature. Wide-angle radiometers become more effective observational tools than scanning (narrow angle) radiometers for some meteorological features between the mesoscale and global dimensions. It is suggested here that the synoptic scale meteorological feature may be the cross over point between the usefulness of scanning and wide-angle radiometers.

The current effort focuses on the problem of interpreting wide-angle observations in terms of the components of the net flux for regions whose dimensions are synoptic scale and larger, i.e., spatial dimensions whose areas are 1-5 x 10^{6} km^{2} to the entire area of the earth. It should be emphasized that this problem of data interpretation is common to both spherical and plate radiometers.

The important point to be noted here is that H_s, W_r, and W_e, can be determined from observational data of satellites orbiting the earth. It follows then, that Q can be computed for any region for which satellite data are available. Consequently, determination of the fluxes W_r and W_e mentioned above for regions smaller than the FOV of the satellite becomes important, and techniques to accomplish this task have been sought for some time.

At Drexel University, two techniques involving matrix inversions were developed for computing the two fluxes under discussion for regions smaller than the FOV. The motivation behind the efforts to determine W_r and W_e for surface areas smaller than the FOV will now be discussed.

Motivation

One can think of two reasons for developing techniques to interpret wide-angle observations for synoptic scale regions. These reasons are:

(a) Knowledge of the radiant energy budget over several areas (such as eastern continental U.S.A., the polar caps, the Northwestern part of Africa, and the Caribbean - Gulf of Mexico region) possessing meteorological significance in the dynamical analysis of the atmosphere are of practical and scientific value. These areas are smaller than the FOV of wide-angle radiometers on satellites at orbital altitudes commonly used.

(b) Several of the regions of interest in studies of the earth's energy budget may have dimensions equal to, or larger than, the FOV of the radiometer (e.g. subtropical oceans). However, often only a portion of the FOV covers part of the area of interest during an observation; and it is, therefore, impossible to determine from this measurement alone what fraction of the power measured originated at the area of concern.

The above arguments provide sufficient reason for endeavoring to develop the types of techniques sought. The essentials of the two techniques developed at Drexel follow.

Essentials of Techniques

In one technique, the number of observations m equals the number n of regions under study, and a unique solution is obtained for each region. The resulting system of n simultaneous equations is solved by operating on the observed power column matrix with the inverse of the configuration factor matrix. If all the observations are made at one time during a single pass of the satellite, the solutions are termed INSTANTANEOUS. For this reason, the technique is called Instantaneous/Inversion Technique.

In the other technique, the number of observations m is larger than the number n of regions being observed. The n simultaneous equations required to seek a solution is obtained by using an extension of the method of least squares to determine the surface which best fits the data. For this reason, this technique is termed the Best Fit/Inversion technique. Again here, the system of n simultaneous equations is solved by the use of a matrix inversion subroutine.

The values of W_e obtained by both techniques from error-free observations were totally acceptable. However, when the measurements included uncertainties, not all the instantaneous values of W_e computed by the first technique were acceptable. Nevertheless, a prediction scheme was developed which forecasts the quality of the instantaneous W_e values to be determined by the first technique. In this scheme, the square matrix of the coefficients of the n simultaneous equations found by the first technique was used to predict the acceptability of the instantaneous values of W_e obtained for each of the regions. The computer program calculates the elements of the matrix and then proceeds to analyze the matrix in order to predict the quality of the data to be obtained. The actual results computed were always compared with the pertinent tolerances listed in TABLE 4-7, Accuracy Requirements for Radiation Budget Components, in order to determine the acceptability of the results. In all cases, the predictions were in agreement with the results of these comparisons. The results obtained by both techniques are now presented.

Accuracy of Results

Two types of errors were selected to perturb the power measurements made by the radiometers. These were, systematic errors (0.3, 0.6, and 0.9 watts/m^2) and gaussian random errors (the gaussian distribution had a sigma value $\sigma = 0.5$ watts/m^2). From TABLE 4-7, the pertinent "desired" and "minimum useful" accuracy requirements for W_e are ±3 watts/m^2 and ±15 watts/m^2, respectively. To evaluate the Instantaneous/Inversion Technique, ten sets of six observations each were included in the analysis. The predictions and the uncertaintities in the values of W_e obtained by using a combination of the gaussian errors mentioned and 0.9 watts/m^2 systematic errors were as follows (refer to TABLE 4-8)

	We_1	We_2	We_3	We_4	We_5	We_6
Predictions, sphere	Poor	Poor	Accept	Accept	Poor	Accept
Prediction, plate	Poor	Poor	Accept	Accept	Reject	Accept
Sphere	15.2	20.1	6.9	3.1	17.4	5.8
Plate	15.4	21.9	9.1	4.2	33.8	9.3

As it can be seen from these results, only the values of We_2 and We_5 exceed significantly the minimum useful accuracy requirements (±15 watts/m^2) given for both satellites in TABLE 4-7. However, it is noticed that consistently the plate exhibits larger uncertaintities than the sphere. It should be remarked here that different satellite orbits that include larger segments within their FOV's of regions one and five would serve to provide W_e values with lesser errors for these regions.

In order to test the Best Fit/Inversion Technique, thrity-six observations of six regions were included. The values of W_e obtained when the power measurements were assumed to exhibit the same combination of errors used above for the Instantaneous/Inversion Technique were as shown below. The six values used as a standard for comparing the values of W_e retrieved were the averages of the given W_e values computed for each of the six-regions.

	We_1	We_2	We_3	We_4	We_5	We_6
Average (Standard)	179.4	200.4	220.4	239.8	259.6	280.4
Results	179.3	200.6	222.2	243.0	257.4	281.5

As it can be seen from these data, the highest uncertainty in the value of W_e is exhibited by We_4, which is 3.2 watts/m^2. However, even this error is below the minimum useful accuracy requirement shown in TABLE 4-7.

BASIC IDEAS

The basic ideas and concepts required for deriving the expression for the total radiant power P (watts) intercepted by a radiometer orbiting the earth are discussed in the following subsections.

Shape or Configuration Factor

This factor F which is dimensionless, appears often in radiative transfer literature and is defined in the following expression (reference 3)

$$P = FAW \tag{2-1}$$

where

P = radiant power (watts) intercepted by the radiometer.

A = characteristic area of the radiometer. This area is $A = \pi a^2$ for both a sphere of radius a and a flat circular plate of radius a.

W = radiant flux (watts/m^2) per unit time, or radiant power per unit area, which is either emitted (radiant emittance W_e) or reflected (radiant reflectance W_r) by the earth-atmosphere (E-A) system.

F = shape, or configuration factor (dimensionless). This factor represents that fraction of an observed area flux W that is intercepted by the radiometer per unit of characteristic area.

The power absorbed by the radiometer is given by,

$$P = \alpha P = \alpha FAW \tag{2-2}$$

where

α = absorptance of the radiometer (dimensionless). It is the ratio of the power absorbed to the power intercepted.

Radiometer Characteristics

Two types of radiometer will be treated in this report: (a) spherical, and (b) horizontal, flat, circular.

The characteristic area $A = \pi a^2$ of both of the above radiometers will be assumed to be $A = 1 m^2$. This assumption serves to simplify the expressions without affecting the physical significance of the results.

Both satellites will be assumed to be blackbodies i.e., the spectral emissivity ε_λ and absorptivity α_λ are assumed to be unity

$$\varepsilon_\lambda = \alpha_\lambda = 1 \tag{2-3}$$

Therefore, all the radiant power P intercepted by either radiometer (sphere or plate) is totally absorbed, and one has

$$P = P_\alpha \tag{2-4}$$

Hence, the power absorbed by the radiometer can be written as

$$P = FW \tag{2-5}$$

Radiance and Radiant Emittance

These two quantities are of great importance in the discussion of long-wave radiation (LWR) emitted by the E-A system. One is interested in the expression that relates the radiance $N(\theta,\psi)$ (watts/m^2 - sr) and the radiant emittance W_e (watts/m^2) of an area element dA(m^2) whose centroid is located at longitude λ and latitude ϕ. The radiance is the radiant power per unit area emitted by dA within an element of solid angle dΩ. The radiant emittance is the total radiant power per unit area (or radiant flux per unit area) emitted by dA into a 2π steradians solid angle. The expression relating the instantaneous values of W_e and N for a given dA (λ,ϕ) is

$$W_e(\lambda,\phi,t) = \int_0^{2\pi} d\psi \int_0^{\pi/2} N(\theta,\psi;\lambda,\phi,t)\sin\theta\cos\theta\, d\theta \tag{2-6}$$

Where the radiance is being considered as a function of the zenith angle θ and the azimuthal angle ψ which define the direction of $N(\theta, \psi; \lambda, \phi, t)$. This quantity and W_e are functions of the position of the area observed as well as of the specific time at which the observation is made. In order to simplify the notation, the dependence of N on λ, ϕ, and t will not be shown.

A reasonable approach in the interpretation of LWR is to assume that the radiance is a function of the zenith angle θ only (reference 4). Then, one can write,

$$N(\theta,\psi) = N(\theta) = N^z f(\theta) \tag{2-7}$$

where N^z = Zenith radiance, i.e., the radiance in the zenith direction, $\theta = 0°$.

$f(\theta)$ = limb darkening function (LDF) which gives a measure of the anisotropy of the radiation field.

Hence, by substituting equation (2-7) into (2-6) one obtains

$$W_e = 2\pi\, N^z \int_0^{\pi/2} f(\theta) \sin\theta \cos\theta \, d\theta \tag{2-8}$$

or

$$N^z = \frac{W_e}{2\pi \int_0^{\pi/2} f(\theta) \sin\theta \cos\theta \, d\theta} \tag{2-9}$$

The integral appearing in (2-8) and (2-9) is used often and hence, it is concenient to define it as,

$$I\,(f) = \int_0^{\pi/2} f(\theta) \sin\theta \cos\theta \, d\theta \tag{2-10}$$

Then, (2-8) and (2-9) can be rewritten as

$$W_e = 2\,\pi\,N^z\,I\,(f)$$

and

$$N^z = \frac{1}{2\pi\ I\ (f)}\ W_e \qquad (2\text{-}11)$$

For an ISOTROPIC radiation field, $f(\theta) = 1$, $I(f) = \frac{1}{2}$, and the isotropic radiance N^{iso} is then

$$N^{iso} = \frac{W_e}{\pi} \qquad (2\text{-}12)$$

Figure 2-1 shows a satellite S at a height H above a spherical E-A system of radius R. The geometric nomenclature to be used in this report is presented in this figure for future reference. A flat earth is depicted tangential to the spherical system at the sub-satellite point(SSP). The concept of a flat earth will be used to make certain calculation simplifications and it will be thoroughly discussed in the subsection entitled "Flat Earth Application". From this figure one can readily write.

$$\theta = \gamma + \alpha$$

$$R \sin\theta = (R + H) \sin\alpha \qquad (2\text{-}13)$$

$$R \sin\gamma = r \sin\alpha \qquad (2\text{-}14)$$

$$r^2 = R^2 + (R + H)^2 - 2R(R+H)\cos\gamma \qquad (2\text{-}15)$$

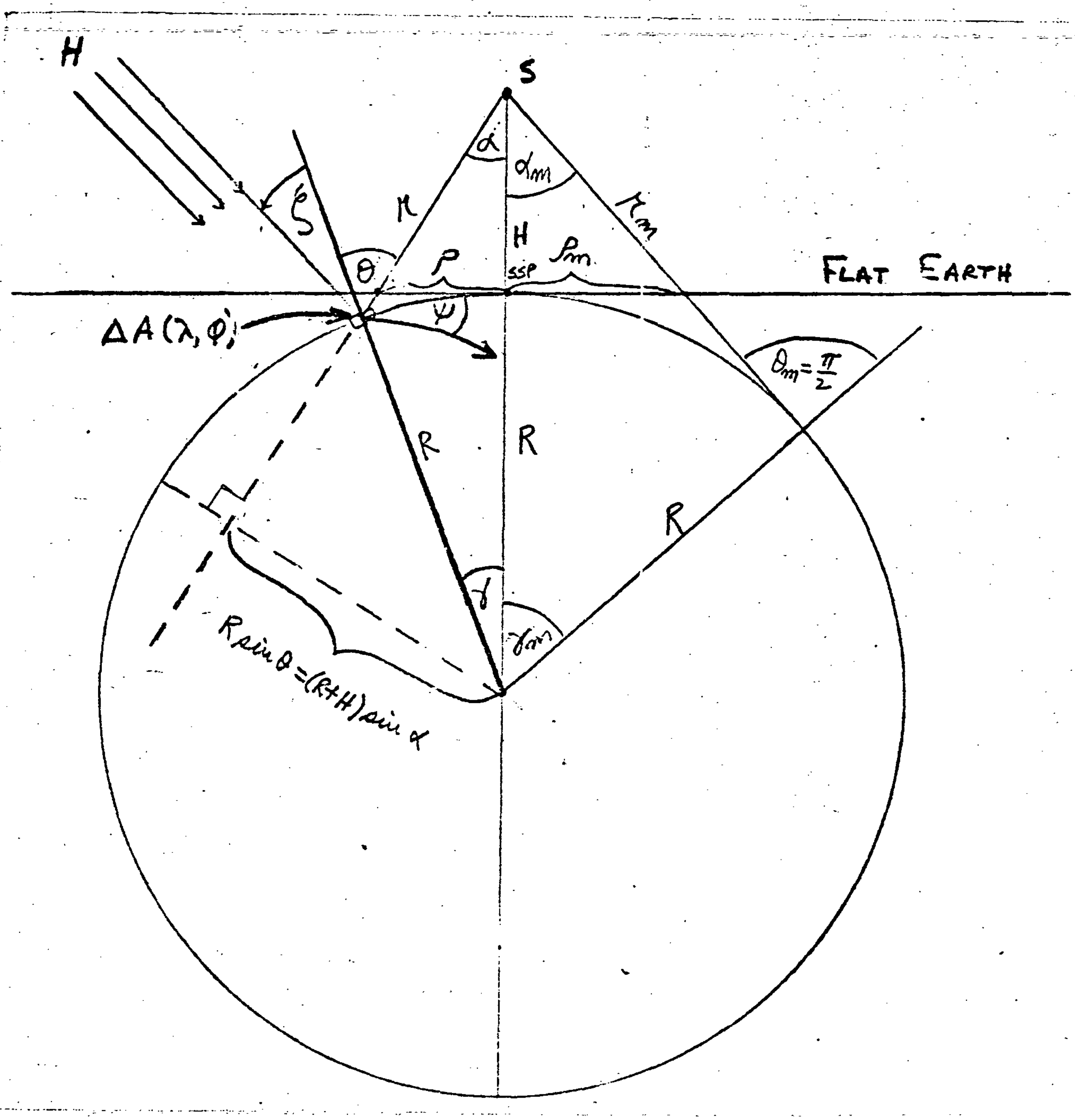

Figure 2-1. Pictorial definition of the symbols used.

Irradiance, Radiance, Radiant Reflectance, and Albedo

These four quantities are of great importance when the solar shortwave radiation (SWR) reflected by the earth is treated. One of the expressions of interest is the relation between the radiance N_r (watts/(m^2- sr)) and the radiant reflectance W_r (watts/m^2) of an area element dA(m^2) whose centroid is located at longitude λ and latitude ϕ. The radiance in this case is the radiant power per unit area reflected by dA within an element of solid angle dΩ. The radiant reflectance is the total radiant power per unit area (or radiant flux per unit area) reflected by dA into a 2π steradians solid angle.

Before writing the expressions connecting N_r and W_r it will prove helpful to define the solar irradiance H (watts/m^2). This is the amount of radiant power per unit area (or radiant flux per unit area) impinging upon dA(λ,ϕ) from all directions contained within a 2π steradians solid angle. Hence, the definitions of W_e, H, and W_r are very similar, except that they refer to emitted, incident, and reflected radiations, respectivley. Then, one can write, using the nomenclature of reference 3.

$$H(L, \zeta, \lambda, \phi, t)=SL \cos \zeta \qquad (2\text{-}16)$$

where

S = Solar constant (S = 1353±21 watts/m^2 = 1.940±.03 cal/(cm^2-min), see reference 5).

L = $\bar{d}^2/d^2$. $\bar{d}$ and d are the mean and true sun-to-earth distances, respectively.

ζ = Zenith angle of the sun at dA (λ,ϕ).

λ = Longitude of the observed area element dA.

ϕ = Latitude of the observed area element dA.

t = specific time at which observation was made.

The instantaneous albedo $A(\zeta,\lambda,\phi,t)$ for the area element $dA(\lambda, \phi)$ is defined by

$$A(\zeta, \lambda, \phi, t)=W_r(L, \zeta, \lambda, \phi, t)/H(L,\zeta,\lambda,\phi,t) \tag{2-17}$$

In order to simplify this expression, one can assume that L does not change significantly during the time interval of the observations. Then, for a given L, the dependence of W_r and H on L does not have to be shown. In a similar way, λ, ϕ, and t can be dropped from the above expressions, and

$$A(\zeta) = W_r(\zeta)/H(\zeta) \tag{2-18}$$

From the definitions given for N_r and W_r at the beginning of this subsection, one can write the following expression relating these two quantities, which is similar to equation (2-8).

$$W_r(\zeta)= \int_0^{2\pi} d\psi \int_0^{\pi/2} N_r(\theta,\psi,\zeta)\sin\theta\cos\theta d\theta \tag{2-19}$$

Dividing this expression through by $H(\zeta)$, one has

$$A(\zeta)= r(\zeta) = \int_0^{2\pi} d\psi \int_0^{\pi/2} \rho(\theta,\psi,\zeta)\sin\theta\cos\theta d\theta \tag{2-20}$$

Where,

$$A(\zeta) = r(\zeta) = \frac{W_r(\zeta)}{H(\zeta)} \tag{2-21}$$

$r(\zeta)$ is the directional reflectance which in this case is the same as the instantaneous albedo.

$$\rho(\theta,\psi,\zeta) = \frac{N_r(\theta,\psi,\zeta)}{H(\zeta)} \tag{2-22}$$

$\rho(\theta,\psi,\zeta)$ is the bidirectional reflectance.

Thus, the directional reflectance is the ratio of the total radiant power per unit area $W_r(\zeta)$ which is reflected by dA onto a 2π steradians solid angle to the total solar radiant power per unit area $H(\zeta)$ incident on dA at a zenith angle ζ. The bidirectional reflectance involves two directions, namely, the direction of the incident radiation which is given by the zenith angle ζ, and the direction of the observer. The latter direction is defined by the zenith angle θ and the azimuthal angle ψ. The bidirectional reflectance is the ratio of that amount of radiant power per unit area per unit solid angle N_r which is reflected by dA onto an element of solid angle $d\Omega\ (\theta,\psi)$ to the total solar radiant power per unit area $H(\zeta)$ incident on dA at the zenith angle ζ.

The integral over the angle θ appearing in equation (2-20) is similar to the one appearing in equations (2-8) and can be treated in a similar manner. That is, one can define $I(\rho)$ as

$$I(\rho) = \int_0^{\pi/2} \rho(\theta,\psi,\zeta)\ \sin\theta\ \cos\theta d\theta \tag{2-23}$$

Then,equation (2-20) can be rewritten as

$$A(\zeta) = r(\zeta) = \int_0^{2\pi} I(\rho)\ d\psi \tag{2-24}$$

A method proposed for utilizing these equations will be discussed at the end of the section entitled Instantaneous/Inversion Technique.

Instantaneous Net Flux

Once the representative values of H, W_r, and W_e are determined for a particular region from a given set of n observations i, taken during a time interval centered at t_j, one can determine the net radiant power, or net flux, $Q_i(t_j)$ for this region. Hence, $Q_i(t_j)$ represents the instantaneous value of the net radiant flux for the specific time of day t_j.

Average Net Flux

It follows from the above discussion of the instantaneous energy budget that a weighted average (using the configuration factor as a weight) for a given region can be obtained from the m values of $Q_i(t_j)$ computed for m sets of observations.

If, for instance, one is interested in obtaining the average of $Q(t_j)$ during a month for a unique value of t_j (say 3:00 PM) from m values, one has

$$Q(t_j) = \frac{\sum_i^m F_i \, Q_i \, (t_j)}{\sum_i^m F_i} \tag{2-25}$$

Other types of averages which are more suitable for the user's needs can be computed in a similar manner.

NOTE: In this report only the LWR component will be treated. The SWR component will be discussed in a subsequent report.

Radiative Equilibrium

When the temperature of the sensor reaches a steady state, it is said that the sensor is in radiative equilibrium. In this state, the power input P_{in} is equal to the power output P_{out}. On the basis of the definition of $N(\theta)$ for the LWR presented in previous sections, one can write the expressions for P_{in} for both satellites, considered as blackbodies, as

$$\text{SPHERE} \qquad P_{in} = A_s \int_0^{2\pi} d\psi \int_0^{\alpha_m} N[\theta(\alpha)] \sin\alpha \, d\alpha \tag{2-26}$$

$$\text{PLATE} \qquad P_{in} = A_s \int_0^{2\pi} d\psi \int_0^{\alpha_m} N[\theta(\alpha)] \sin\alpha \cos\alpha d\alpha \tag{2-27}$$

where α_m is the maximum value of the nadir angle.

The expression for P_{out} for both satellites follows from Stefan-Boltzmann law,

$$\text{SPHERE} \qquad P_{out} = S\,\sigma\,T^4 = 4\,A_s\,\sigma\,T^4 \tag{2-28}$$

$$\text{PLATE} \qquad P_{out} = A_s\,\sigma\,T^4 \tag{2-29}$$

Where, $\sigma = 5.6697\text{x}10^{-8}$ watts/(m^2-$^oK^4$); Stefan-Boltzmann constant.

It will be assumed only for convenience that the characteristic areas of both radiometers is $A_s = 1m^2$. Also, $N[\theta(\alpha)]$ will be written in terms of N^z and $f[\theta(\alpha)]$ per equation (2-7).

Then, the above four equations can be rewritten as, SPHERE $$P_{in} = 2\pi N^z \int_o^{\alpha_m} f[\theta(\alpha)] \sin \alpha d\alpha \tag{2-30}$$

PLATE $$P_{in} = 2\pi N^z \int_o^{\alpha_m} f[\theta(\alpha)] \sin \alpha \cos \alpha d\alpha \tag{2-31}$$

SPHERE $$P_{out} = 4 \sigma T^4 \tag{2-32}$$

PLATE $$P_{out} = \sigma T^4 \tag{2-33}$$

Substituting in (2-30) and (2-31) the value of N^z as given by (2-9), one obtains,

SPHERE $$P_{in} = \frac{\int_o^{\alpha_m} f[\theta(\alpha)] \sin \alpha \, d\alpha}{\int_o^{\pi/2} f(\theta) \sin \theta \cos \theta \, d\theta} W_e \tag{2-34}$$

PLATE $$P_{in} = \frac{\int_o^{\alpha_m} f[\theta(\alpha)] \sin \alpha \cos \alpha \, d\alpha}{\int_o^{\pi/2} f(\theta) \sin \theta \cos \theta \, d\theta} W_e \tag{2-35}$$

But comparing equation (2-5), that is $P = FW$, with equations (2-34) and (2-35) one sees that the expressions for the shape factors for both radiometers are

$$F_{sph} = \frac{\int_0^{\alpha_m} f[\theta(\alpha)] \sin\alpha \, d\alpha}{\int_0^{\pi/2} f(\theta) \sin\theta \cos\theta \, d\theta} \tag{2-36}$$

$$F_{pl} = \frac{\int_0^{\alpha_m} f[\theta(\alpha)] \sin\alpha \cos\alpha \, d\alpha}{\int_0^{\pi/2} f(\theta) \sin\theta \cos\theta \, d\theta} \tag{2-37}$$

or, using the definitin of I(f) given by (2-10), one can write

$$F_{sp} = \frac{1}{I(f)} \int_0^{\alpha_m} f[\theta(\alpha)] \sin\alpha \, d\alpha \tag{2-38}$$

$$F_{pl} = \frac{1}{I(f)} \int_0^{\alpha_m} f[\theta(\alpha)] \sin\alpha \cos\alpha \, d\alpha \tag{2-39}$$

For the special case of isotropic radiation

$f[\theta(\alpha)] = 1$ and $I(f) = \frac{1}{2}$. Then,

$$F_{sp}^{iso} = 2(1 - \cos\alpha_m) \tag{2-40}$$

$$F_{pl}^{iso} = \sin^2 \alpha_m \tag{2-41}$$

FUNDAMENTALS OF THE TECHNIQUES

The only piece of information that a single satellite observation can yield is the total radiant power intercepted by the radiometer, as given by either equation (2-30) for a sphere, or (2-31) for a plate. This power represents the sum of those radiances originating at each of the area elements within the FOV and directed toward the radiometer. Therefore, it is impossible to obtain from a single, wide-angle measurement, and without additional information of any kind, an exact or rigorous solution for either W_e or W_r for any area within the FOV of the radiometer.

A similar situation exists for measurements by narrow-angle radiometers. The only information that is contained in a single observation of an area element is the radiance in the direction of the radiometer on the satellite. Scanning by this radiometer only adds information about adjacent area elements and nothing additional about the original area element under consideration. Hence, the fundamental difficulty one faces when trying to determine the W_e field from a measurement of the radiance N (or W_r from N_r) is that the total angular distribution of N (or N_r) can not be deduced from the measurement, and hence, W_e can not be deduced from the measurement either.

It follows from the above discussion that it is impossible to determine the W_e (or W_r) field of an area of any size - i.e., of an area smaller than the FOV, equal to the FOV, or larger than the FOV of the radiometer - unless the angular distribution of N is also made availalbe. On the other hand, it is possible that by utilizing representative values of the angular distributions of N and N_r obtained from previous observations the problem can be rendered solvable in a satisfactory manner. Furthermore, these angular distribution values can be refined in the future by increasing the number of measurements of these distributions for different regions of the E-A system, as well as by improving the accuracy and precision of these measurements.

Therefore, one can utilize an empirical model which portrays the angular emitting and reflecting characteristics of the E-A system, based on previous observations (satellite, aircraft, etc.) in order to solve the problem. At Drexel University, this approach was followed by making certain assumptions which are justifiable on the basis of physical processes and observational data accumulated by other investigators (reference 4). These assumptions are discussed in the following subsection.

Basic Assumptions

The following basic assumptions were sufficient to develop a technique for computing W_e and W_r from radiant power measurements taken by spherical and horizontal flat circular radiometers.

Division into regions. The surface area of the earth - atmosphere system is assumed divisible into regions which have emitting and reflecting characteristics significantly distinct from those of adjacent regions. The criterion for implementing the division must ultimately be based on results of previous satellite observations. The values of W_e and W_r computed for a given region are considered to represent the mean of the meteorological variations taking place in the time interval Δt(e.g., a month) during which the observations were made.

Position and extent of each region. The position and extent of each region is assumed to be available or can be approximated from data gathered by previous investigators.

Angular distribution of N and N_r. The angular dependence of N for LWR, and of N_r for the reflected solar SWR are available, or approximations can be made, from previous observations.

Although two different techniques for computing the radiant emittance and radiant reflectance fields have been developed at Drexel, the initial computational steps are common to both techniques. These common steps are discussed in detail in the following subsection.

Mathematical Bases

In this subsection, the mathematical bases which are common to both techniques are treated in detail. At the end of the subsection, the principal differences in the two techniques for accomplishing the final goal are listed.

The problem to be solved is illustrated in figure 3-1, which depicts a satellite (which for simplification is assumed to be crossing the equator) with three different regions (R_1, R_2, and R_3) falling, partially or totally, within the FOV of its radiometer. The following development is for a spherical radiometer; however, the treatment for horizontal flat sensor is similar.

A spherical radiometer of unit cross-sectional area is considered. Using $P = FW$, as given by equation (2-5), one can write for the total power contributed by those portions of the three regions within the FOV of a radiometer on board the satellite at position S in figure 3-1 the following,

$$P_{in} = P_1 + P_2 + P_3 \tag{3-1}$$

or

$$P_{in} = F_1 W_{e1} + F_2 W_{e2} + F_3 W_{e3} \tag{3-2}$$

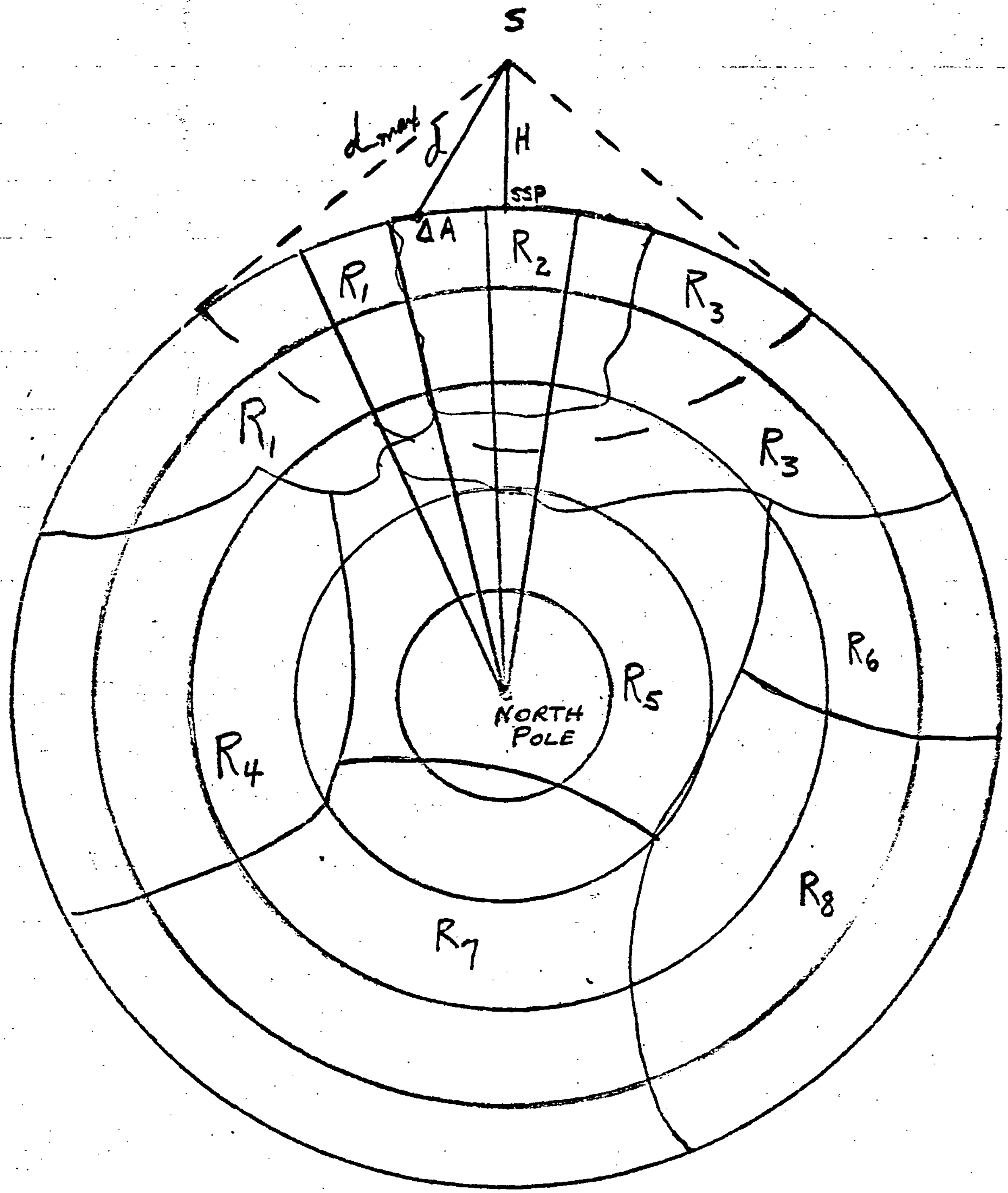

Figure 3-1. Regions within the FOV of a satellite crossing the equator.

That is, by using (2-30) to represent the power originating at region R_1 and which is intercepted by the satellite, one can write

$$P_1 = F_1 W_{e1} = N_1^z \int_{\psi_{1\ell}}^{\psi_{1n}} d\psi \int_{\alpha_{1\ell}}^{\alpha_{1u}} f_1[\theta(\alpha)]\sin\alpha \, d\alpha \qquad (3\text{-}3)$$

Where,

P_1 = radiant power from region R_1 intercepted by the radiometer.

N_1^z = zenith radiance of region R_1.

$\psi_{1\ell}$ = lower boundary for ψ in region R_1.

ψ_{1n} = upper boundary for ψ in region R_1.

$\alpha_{1\ell}$ = lower boundary for α in region R_1.

α_{1n} = upper boundary for α in region R_1.

To facilitate the discussion, an isotropic radiation field will be assumed. Hence, $f[\theta(\alpha)] = 1$, and one obtains

$$P_1 = F_1 W_{e1} = N_1^{iso} \int_{\psi_{1\ell}}^{\psi_{1u}} d\psi \int_{\alpha_{1\ell}}^{\alpha_{1u}} \sin\alpha \, d\alpha \qquad (3\text{-}4)$$

Where

N_1^{iso} = Isotropic radiance of region R_1.

Using expressions similar to (3-4) for P_2 and P_3 we can rewrite (3-1) for the power input to the radiometer, as

$$P = N_1^{iso} \int_{R_1} d\psi \int_{R_1} \sin\alpha \, d\alpha + N_2^{iso} \int_{R_2} d\psi \int_{R_2} \sin\alpha \, d\alpha + N_3^{iso} \int_{R_3} d\psi \int_{R_3} \sin\alpha \, d\alpha \qquad (3\text{-}5)$$

Where R_1, R_2, and R_3 imply that the integration limits are those corresponding to the regions 1,2, and 3, respectively.

Equation (3-5) can be rewritten as

$$P = \sum_{i=1}^{3} N_i^{iso} \iint_{R_i} \sin \alpha \, d\alpha \, d \psi \tag{3-6}$$

By using equation (2-12), P can be expressed in terms of W_{ei} rather than N_i^{iso}, that is,

$$P = \frac{1}{\pi} \sum_{i=1}^{3} W_{ei} \iint_{R_i} \sin \alpha \, d\alpha \, d \psi \tag{3-7}$$

The main problem at this point is to decide which is the most advantageous and efficient manner to perform the integration indicated in equations (3-6) or (3-7).

Two main approaches were considered; these are discussed in the following paragraphs together with the advantages that each presents.

The following different methods were considered.

(a) The integrations indicated in equation (3-6) could be performed numerically (e.g., by using the trapezoidal rule) between the boundaries given for each region in terms of longitude and latitude.

(b) The integrations could be performed geometrically. That is, by dividing the surface area of the E-A system into a large number L of area elements, one could simply sum up the radiances that each of the area elements emits in the direction of the satellite in order to accomplish the integration indicated by (3-6).

It was decided that the second approach was more advantageous for the following reasons:

(a) In the first approach, since the boundaries of the regions do not necessarily follow longitudinal and latitudinal lines of constant value, the number of separate integrations to be performed could often be impractically high. Furthermore, the limits of integration for the angles α and ψ could involve difficult trigonometric expressions which could make the implementation of this procedure highly impractical.

(b) In the second method, once the centroids and boundaries of each of the area elements have been accurately defined, the regions can be easily defined in terms of a group of adjacent area elements.

(c) In the second method, a procedure for testing whether a particular area element ΔA should be considered to be within the FOV or not can be easily implemented if the longitude and latitude of the centroid of ΔA is known. If the centroid is on, or inside of the perimeter of the FOV, ΔA is considered to be within the FOV; otherwise, it is considered to be outside the FOV. On the average, it is expected that as many area elements will be accepted as will be rejected in each integration. Furthermore, since it is at the limb that the area elements are tested to be accepted or rejected, and since these area elements have much smaller shape factors than those situated close to the SSP, it is clear that the error would be negligible even if the number of area elements accepted do not match the number rejected.

Therefore the second method will be followed in which the surface of the E-A system is divided into a large number L of area elements ΔA, and each area element is identified by the longitude and latitude of its centroid.

In order to illustrate the computation of the radiant power intercepted by a satellite radiometer whose FOV comprises more than one region, a FLAT E-A system will be assumed. This type of system greatly simplifies the results. Only three regions and three FOV's will be considered, which are depicted in figure 3-2. The portion of the flat E-A system shown in this figure is comprised between 0^o and 70^o longitude, and between -50^o and $+50^o$ latitude, which is adequate for the purposes of this discussion. An area element is considered within the FOV if its centroid lies on, or within, the perimeter of the FOV, as per the criterion stated earlier. In figure 3-2, the area elements have been numbered in order to identify them more easily. In TABLE 3-1, the elements that are considered to be contained in each of the three FOV's are tabulated. It is seen that in this instance, each FOV contains exactly twenty-six area elements.

The equations used to calculate the radiant power that an area element $\Delta \bar{A}$ contributes to one observation are presented below. The symbols entering in these expressions are shown in figure 3-3 which is a schematic of a radiometer at a position S over the flat E-A system.

Let ΔP_{ijk} be the power that the ith area element in the kth region contributes to the jth observation. Then, one writes for a <u>spherical radiometer</u>

$$\Delta P^{S}_{ijk} = N_{ijk} \Delta A_{ijk} \cos \theta_{ijk} \frac{A_s}{d^2_{ijk}} \tag{3-8}$$

For a <u>horizontal flat circular radiometer</u>, one writes,

$$\Delta P^{P}_{ijk} = N_{ijk} \Delta A_{ijk} \cos \theta_{ijk} \frac{A_s \cos \alpha_{ijk}}{d^2_{ijk}} \tag{3-9}$$

N_{ijk} = Radiance of ΔAi in the direction of the radiometer

A_s = Characteristic area of the satellite radiometer, which for the sphere and plate is πa^2 (a = radius of sphere and plate).

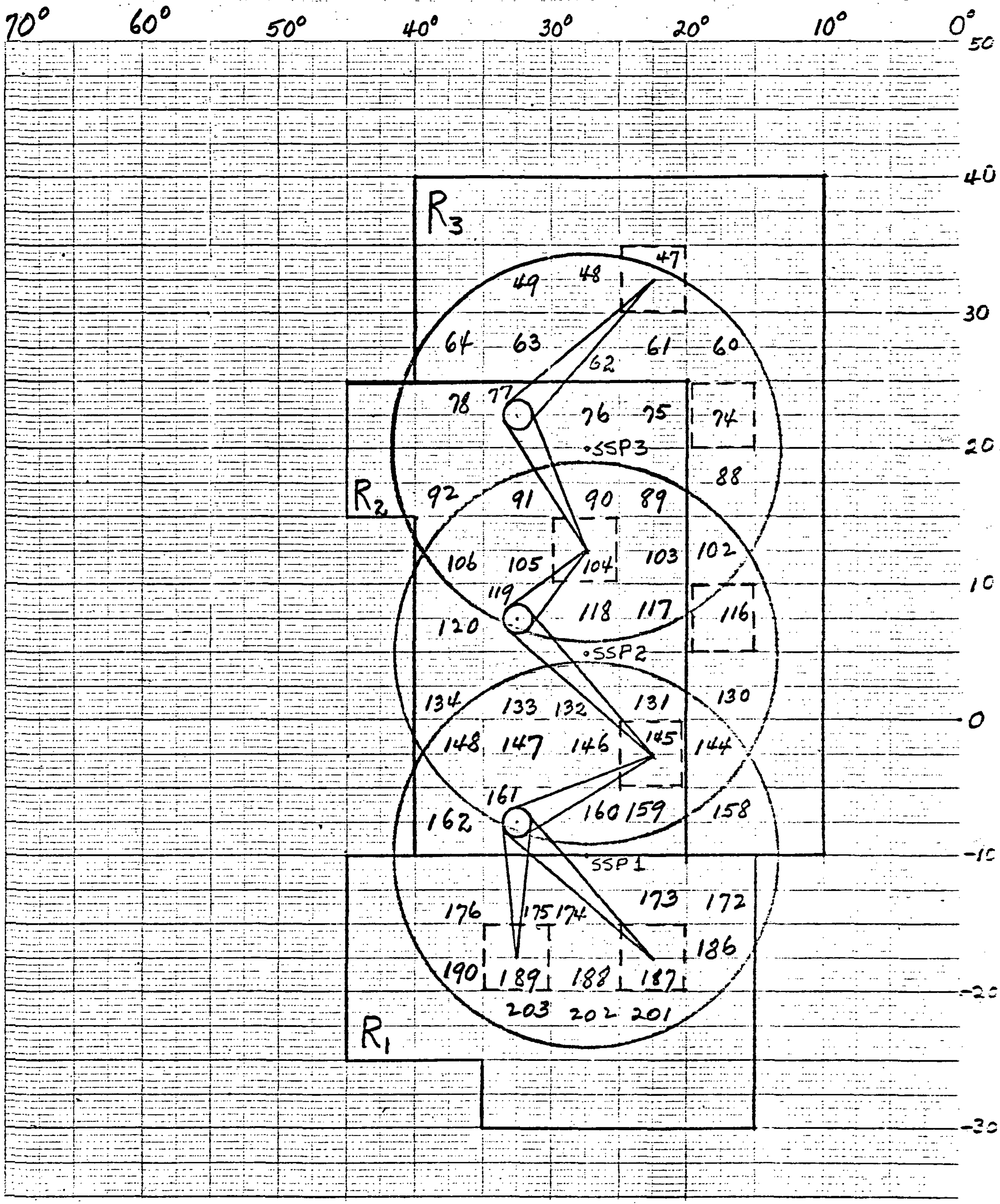

Figure 3-2. Three satellite positions over three regions.

TABLE 3-1. Data from three satellite observations.

Observation No.	Region No.	Area Element No.	No. of Elements	Elements Per Obs.
1	1	201-203	3	
1	1	186-190	5	
1	1	172-176	5	
1	3	158	1	
1	2	159-162	4	
1	3	144	1	
1	2	145-148	4	
1	2	131-133	3	26
2	2	159-161	3	
2	3	144	1	
2	2	145-148		
2	3	130	1	
2	2	131-134	4	
2	3	116	1	
2	2	117-120	4	
2	3	102	1	
2	2	103-106	4	
2	2	89-91	3	26
3	2	117-119	3	
3	3	102	1	
3	2	103-106	4	
3	3	88	1	
3	2	89-92	4	
3	3	74	1	
3	2	75-78	4	
3	3	60-64	5	
3	3	47-49	3	26

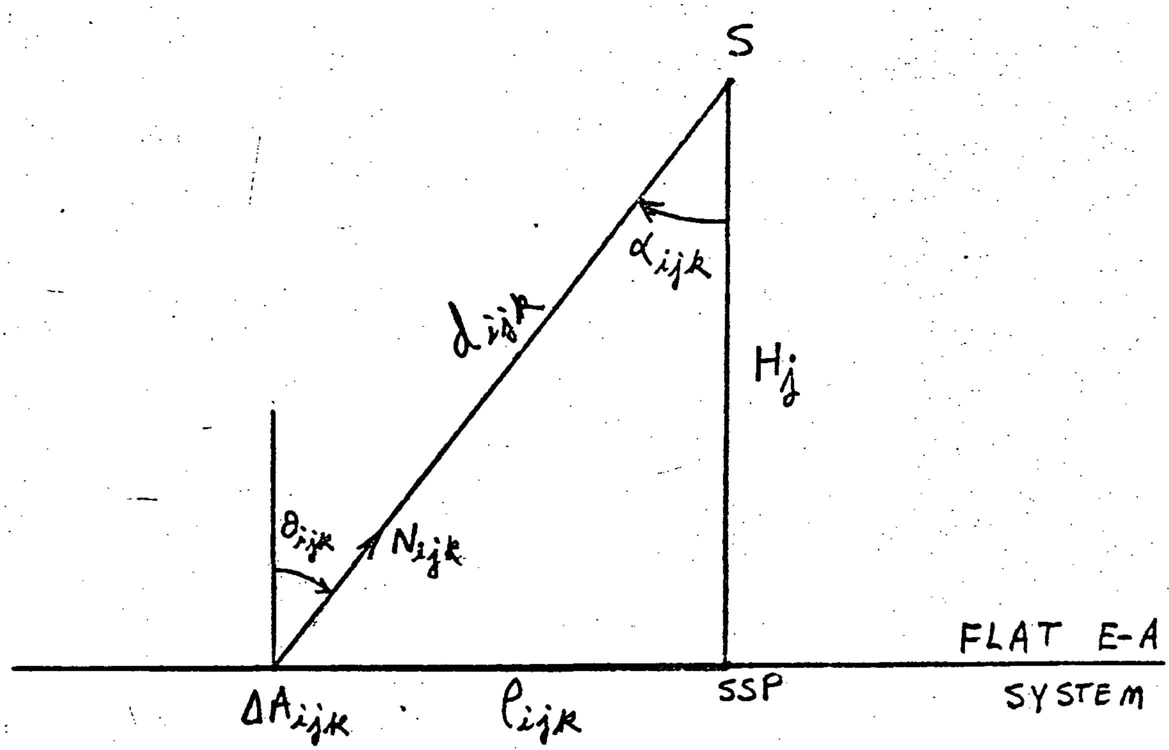

Figure 3-3. Radiance N_{ijk} emitted by ΔA_{ijk} of a flat E-A system and intercepted by the radiometer S.

ΔA_{ijk} = ith area element in the kth region within the FOV of the jth observation.

θ_{ijk} = Zenith angle of the radiometer at ΔA_{ijk}

α_{ijk} = Nadir angle of ΔA_{ijk} at the radiometer

d_{ijk} = Distance from ΔA_{ijk} to the radiometer

Let it be assumed that N_{ijk} is a function of the zenith angle θ_{ijk} only (i.e., that it is independent of the azimuthal angle ψ_{ijk}). Then, one can write

$$N_{ijk} = N_{ijk}^{z} f(\theta_{ijk}) \tag{3-10}$$

Where,

N_{ijk}^{z} = radiance in the zenith direction at ΔA_{ijk}

$f(\theta_{ijk})$ = limb darkening function (LDF) or anisotropic factor at ΔA_{ijk}

It will be further assumed that a region K is characterized by the following:

(a) The value of the LWR radiant emittance in the kth region has a representative average value W_{ek}.

(b) The LWR radiance in the zenith direction has also a representative average value N_k^z in the kth region.

(c) The LDF has a representative functional form $f_k(\theta)$ throughout the kth region.

Hence, for the kth region one rewrites (3-10)as

$$N_{ijk} = N_k^z f_k (\theta_{ijk}) \tag{3-10'}$$

To avoid carrying A_s in the following expressions, it is assumed that $A_s = 1\ m^2$. This assumption does not affect the validity of the results. By substituting (3-10) into (3-8) and (3-9), and making $A_s = 1 m^2$, one obtains,

$$\Delta P^{s}_{ijk} = N^{z}_{k}\ f_k\ (\theta_{ijk}) \Delta A_{ijk} \cos\theta_{ijk} \frac{1}{d^2_{ijk}} \tag{3-11}$$

$$\Delta P^{p}_{ijk} = N^{z}_{k}\ f_k\ (\theta_{ijk}) \Delta A_{ijk} \cos\theta_{ijk} \frac{\cos\alpha_{ijk}}{d^2_{ijk}} \tag{3-12}$$

In the section BASIC IDEAS, the following expressions were introduced to show the relationship between N^z_k and W_{ek}. From equations (2-10) and (2-11) one then writes, respectively,

$$I(f_k) = \int_0^{\pi/2} f_k(\theta) \sin\theta \cos\theta\ d\theta \tag{3-13}$$

$$N^z_k = \frac{1}{2\pi\ I\ (f_k)}\ W_{ek} \tag{3-14}$$

Substituting (3-14) into (3-11) and (3-12) one obtains,

$$\Delta P^{s}_{ijk} = \left[\frac{f_k(\theta_{ijk})}{2I\ (f_k)}\right]\left[\frac{\Delta A}{\pi}\right] \frac{\cos\theta_{ijk}}{d^2_{ijk}}\ W_{ek} \tag{3-15}$$

$$\Delta P^{p}_{ijk} = \left[\frac{f_k(\theta_{ijk})}{2I\ (f_k)}\right]\left[\frac{\Delta A}{\pi}\right] \frac{\cos\theta_{ijk}\ \cos\alpha_{ijk}}{d^2_{ijk}}\ W_{ek} \tag{3-16}$$

Although the subscripts in ΔA_{ijk} identify the position, the observation, and the region, respectively, of the area element under consideration, these subscripts can be dropped here since they appear in other variables in the same expression. Also, the magnitude of ΔA has been assumed to be the same for all area elements; and hence, it is unnecessary to identify it with the subscripts.

It was shown in expression (2-5) that if $A_s = 1m^2$, the power P is related to the radiant emittance W_e by means of the shape factor F, that is

$$P = F\ W_e \tag{3-17}$$

Hence, using the definition of the shape factor, one obtains from (3-15) and (3-16),

$$F^s_{ijk} = \left[\frac{f_k(\theta_{ijk})}{2I\ (f_k)}\right]\left[\frac{\Delta A}{\pi}\right]\frac{\cos\ \theta_{ijk}}{d^2_{ijk}} \tag{3-18}$$

$$F^p_{ijk} = \left[\frac{f_k(\theta_{ijk})}{2I\ (f_k)}\right]\left[\frac{\Delta A}{\pi}\right]\frac{\cos\ \theta_{ijk}\ \cos\ \alpha_{ijk}}{d^2_{ijk}} \tag{3-19}$$

From figure 3-3, it is seen that for a <u>flat</u> E-A system (which is the type of system being used in this development) d^2_{ijk} is given by

$$d^2_{ijk} = H^2 + \rho^2_{ijk} \tag{3-20}$$

which is different from the equivalent expression for a spherical E-A system, which from figure 2-1 can be seen to be

$$r^2_{ijk} = R^2 + (R+H)^2 - 2R(R+H)\cos\ \gamma \tag{3-21}$$

where,

r_{ijk} = distance from ΔA_{ijk} to the radiometer in the spherical E-A system.

R = radius of the E-A system.

γ = angle between A_{ijk} and the SSP, measured at the center of the earth.

In order to obtain the power P_{jk} contributed by the kth region to the jth observation of both, the sphere and the plate, equations (3-15) and (3-16) are summed up over i.

$$P^s_{jk} = \sum_{i=1}^{I} \Delta P^s_{ijk} = \sum_{i=1}^{I} F^s_{ijk} W_{ek} \tag{3-22}$$

$$P^p_{jk} = \sum_{i=1}^{I} \Delta P^p_{ijk} = \sum_{i=1}^{I} F^p_{ijk} W_{ek} \tag{3-23}$$

where,

I = total number of area elements ΔA_{ijk} of the kth region that were under the FOV of the jth observation.

Similarly, the configuration factor F_{jk} represents the contribution by the kth region to the jth observation and is obtained as follows,

$$F^s_{jk} = \sum_{i=1}^{I} F^s_{ijk} \tag{3-24}$$

$$F^p_{jk} = \sum_{i=1}^{I} F^p_{ijk} \tag{3-25}$$

And for the three contributions from the regions R_k (k = 1,2,3) to the jth observation one obtains by combining (3-22) with (3-24) and (3-23) with (3-25),

$$P^s_j = \sum_{k=1}^{3} P^s_{jk} = \sum_{k=1}^{3} F^s_{jk} W_{ek} \qquad (3\text{-}26)$$

$$P^p_j = \sum_{k=1}^{3} P^p_{jk} = \sum_{k=1}^{3} F^p_{jk} W_{ek} \qquad (3\text{-}27)$$

Or, writing in detail these expressions, one obtains for the sphere,

$$P^s_1 = F^s_{11} W_{e1} + F^s_{12} W_{e2} + F^s_{13} W_{e3}$$

$$P^s_2 = F^s_{21} W_{e1} + F^s_{22} W_{e2} + F^s_{23} W_{e3} \qquad (3\text{-}28)$$

$$P^s_3 = F^s_{31} W_{e1} + F^s_{23} W_{e2} + F^s_{33} W_{e3}$$

And for the plate one has,

$$P^p_1 = F^p_{11} W_{e1} + F^p_{12} W_{e2} + F^p_{13} W_{e3}$$

$$P^p_2 = F^p_{21} W_{e1} + F^p_{22} W_{e2} + F^p_{23} W_{e3} \qquad (3\text{-}29)$$

$$P^p_3 = F^p_{31} W_{e1} + F^p_{32} W_{e2} + F^p_{33} W_{e3}$$

By denoting the matrix of the coefficients for the sphere and plate, respectively, as F^s and F^p, one can express (3-28) and (3-29) in matrix form as follows,

$$F^s \{ W_e \} = \{ P^s \} \qquad (3\text{-}30)$$

$$F^p \{ W_e \} = \{ P^p \} \qquad (3\text{-}31)$$

Where, $\{W_e\}$ is the column matrix of the radiant emittance whose elements are the We_k (k - 1,2,3) values of the three regions. $\{P^s\}$ and $\{P^p\}$ are column matrices whose elements are the individual power measurements by the spherical and flat radiometers, respectively.

The mathematical expressions presented up to this point are common to both of the techniques developed at Drexel. From this point on the two techniques proceed by different paths. The fundamentals of these two techniques will be broadly discussed in the next paragraphs before proceeding to the next sections in which each of the techniques and the results obtained by applying them are discussed in detail.

Instantaneous/inversion technique. In this technique, the number m of observations matches the number of regions n (i.e., the n unknown values of W_e), and hence, the solutions are unique. It is termed instantaneous since the procedure is implemented by taking all the m=n observations during one single pass or orbit of the satellite. Several sets of instantaneous results obtained at different time intervals can be grouped together and weight-averaged over the complete time period comprising the total number of observations. The weights to be used are the configuration factors of those region segments appearing within each of the FOV's, or the areas of the region segments.

Therefore, in this procedure, the solution to the n simultaneous equations of the type shown in the set of equations (3-22) for n=3 can be accomplished by inverting the configuration factor matrix. The inverted matrix then, when multiplied by the column matrix of the n power measurements P_j yields the n We_k values one seeks.

Best-fit/inversion technique. In this technique, the number of observations m is larger than the number of regions n (i.e., the n unknown values of W_e). The n simultaneous equations required to solve the problem are obtained by using an extension of the method of least squares. These n simultaneous equations are solved by using a matrix inversion subroutine. The n We_k values determined in this manner represent the partial coefficients of a surface which best fits the data resulting from the observations. These W_e represent a mean atmospheric situation portraying the overall condition for a significantly large time period (e.g., a month), and no instantaneous results are ever obtained from application of this technique. Here again, each of the m observations will be represented by an expression similar to those shown in the set of equations (3-26) or (3-27).

The details of this procedure are presented by means of an illustration in the section entitled "Best Fit/Inversion Techniques."

INSTANTANEOUS/INVERSION TECHNIQUE

A mathematical technique for computing the value of W_e will first be presented. Afterwards, the technique will be tested by applying it to a simplified case of a flat E-A system.

Mathematical Development

The set of simultaneous equations (3-28) for the case of n unknowns can be written in matrix form as follows

$$\{P\} = F\ \{W_e\} \tag{4-1}$$

where

$\{P\}$ = column matrix whose elements are the n power measurements

$\{W_e\}$ = column matrix whose elements are the hypothetical values of W_e for each of the n regions

F = n by n configuration factor matrix whose elements F_{jk} are given by (3-18), and which can be written as,

$$F = \begin{Vmatrix} F_{11} & F_{12} & \cdots & F_{1n} \\ F_{21} & F_{22} & \cdots & F_{2n} \\ \vdots & & & \\ F_{n1} & F_{n2} & \cdots & F_{nn} \end{Vmatrix} \tag{4-2}$$

F^{-1}, the inverse of F, is then computed in order to solve equations (4-1) for W_e by operating with F^{-1} on $\{P\}$, that is,

$$F^{-1}\ \{P\} = \{W_e\} \tag{4-3}$$

So far, it has been tacitly assumed that F and {P} are <u>exact</u> (i.e., do not contain errors). Now, however, it will be assumed that the observations {P} include uncertainties {δP}.

Then, the actual equation to be solved is not the exact equation (4-1) but the perturbed equation (reference 6)

$$F \{W_e'\} = \{P + \delta P\} \tag{4-4}$$

where $\{W_e'\}$ has been introduced to represent the exact solution of the perturbed equation (4-4) as opposed to $\{W_e\}$ which is the exact solution of the <u>exact equation</u> (4-1). One can then write

$$\{W_e'\} = \{W_e + \delta W_e\} \tag{4-5}$$

Again, using the inverse of F one obtains from (4-4) and (4-5),

$$F^{-1}\{P + \delta P\} = \{W_e + \delta W_e\} \tag{4-6}$$

or,

$$F^{-1}\{P\} + F^{-1}\{\delta P\} = \{W_e\} + \{\delta W_e\} \tag{4-7}$$

Subtracting (4-3) from (4-7) one obtains

$$F^{-1}\{\delta P\} = \{\delta W_e\} \tag{4-8}$$

If the elements of the error matrix $\{\delta W_e\}$ are large for small error elements {δP}, the perturbed equation (4-4) is known as ILL-CONDITIONED, the INVERSE MATRIX F^{-1} is termed UNSTABLE, and the matrix F is called ILL-CONDITIONED (references 6 and 7).

If the elements of $\{\delta W_e\}$ are small, or acceptable according to some prescribed accuracy requirements, then expression (4-8) has solved the problem of retrieving the values of W_e, and nothing else needs to be done. On the other hand, if the resulting elements of $\{\delta W_e\}$ do not meet the accuracy requirements for a given set of small uncertainties $\{\delta P\}$, then the problem has just begun. This is the situation that will be treated in the following paragraphs.

Let it be assumed that the elements of $\{\delta W_e\}$ are unacceptable, but that the unstable matrix F^{-1} can somehow be modified to become a stable matrix $\tilde{F}^{-1}$, which, when operating on $\{\delta P\}$, yields a set of new errors in W_e which are now acceptable. These errors $\delta\tilde{W}_e$ are the elements of the new column matrix $\{\delta W_e\}$ resulting from the following equations.

$$\tilde{F}^{-1}\{P + \delta P\} = \{W_e + \delta\tilde{W}_e\} \tag{4-9}$$

or,

$$\tilde{F}^{-1}\{P\} + \tilde{F}^{-1}\{\delta P\} = \{W_e\} + \{\delta\tilde{W}_e\} \tag{4-10}$$

But it is known that $\{W_e\}$ is related to the exact power column matrix $\{P\}$ by (4-3). That is

$$\{W_e\} = F^{-1}\{P\} \tag{4-11}$$

Subtracting (4-11) from (4-10) one obtains,

$$\tilde{F}^{-1}\{P\} - F^{-1}\{P\} + \tilde{F}^{-1}\{\delta P\} + \{\delta\tilde{W}_e\} \tag{4-12}$$

or

$$[\tilde{F}^{-1} - F^{-1}]\{P\} + \tilde{F}^{-1}\{\delta P\} = \{\delta\tilde{W}_e\} \tag{4-13}$$

Equation (4-13) shows that the new inverse matrix can contribute in the following two ways to the value of $\{\delta W_e\}$.

(a) The n by n matrix resulting from subtracting the old inverse matrix from the new one appears multiplying the power matrix $\{P\}$.

(b) The new n by n inverse matrix $\tilde{F}^{-1}$ multiplies the power uncertainty matrix $\{\delta P\}$.

In the subsection entitled "Matrix Stabilization," a detailed account of a scheme found to stabilize the inverse matrix F^{-1} is given. In that subsection is also explained the physical significance of modifying the unstable inverse matrix.

In order to implement this technique, a computer program would be required for performing the numerical integrations, matrix inversions, matrix stabilizations, and tests that would be deemed necessary. Furthermore, another computer program would be required for dividing the surface of the spherical earth-atmosphere system into a finite number of area elements. The output data of the latter program would be used in the former for accomplishing the numerical integrations.

Nevertheless, before engaging in writing these large and sophisticated computer programs, it was decided to subject the technique to a test. By considering a hypothetical flat earth-atmosphere system, some of the equations, as well as the overall computer program could be greatly simplified. On the other hand, the procedure developed to stabilize the inverses of the matrices would be rigorously tested. In the next subsection, the flat E-A system is discussed.

Flat Earth Application

By considering the E-A system to be flat rather than spherical, the task was greatly simplified and less time consuming while the results obtained can be interpreted as a representation of actual physical situations in a spherical system. This flat E-A system was assumed to be a rectangle of 360° of longitude by 180° of latitutde. The longitude is measured westward (to the left) from 0°, at a hypothetical Greenwich meridian, to 360°. The latitude is measured northward (upward) from 0°, at a hypothetical equator, to 90°; and southward (downward) from 0° to -90°. It was found convenient, for interpreting some of the results, to consider the flat E-A system to be tangential to the spherical E-A system at the SSP, as shown in figure 4-1. At any point in this flat E-A system, one degree of longitude is the same as one degree of latitude and each is equal to 100 km. The surface area of this system was divided into a total of 2592 equal area elements ΔA of 5° by 5°. The area of an area element is given by ΔA = 500 km x 500 km = 250,000 km^2 = $2.5x10^{11}m^2$. The surface area of the system was also divided into 162 regions of 20° by 20°, or 2000 km by 2000 km. It is to be noted that the area elements are used to perform the numerical or geometrical summations or integrations. Each area element ΔA is identified by the longitude and latitude of its centroid, and hypothetical values of W_e and albedo can be assigned to ΔA. However, in the present report only W_e is included. Direct and reflected SWR will be discussed in a subsequent report. A region is characterized by a representative value of W_e (and/or $W_r(0)$), and variations of W_e (or $W_r(0)$) within it are neglibibly small or undetectable by a radiometer.

The radius ρ of that area of the flat E-A system within the FOV of the radiometer can be quickly claculated with the aid of figure 4-1. From this figure, it can be seen that

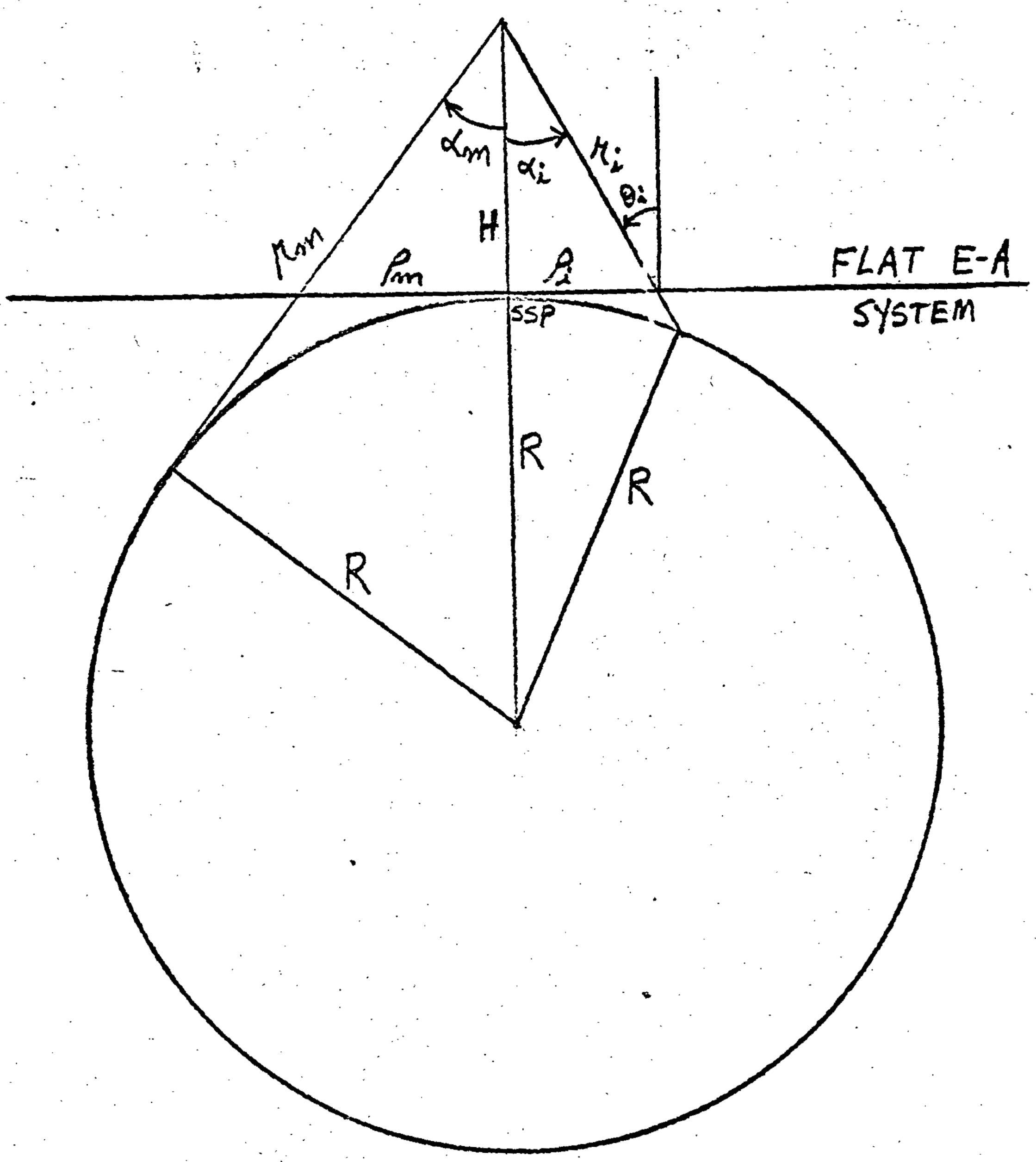

Figure 4-1. Flat E-A system parameters.

$$\alpha_m = \sin^{-1}\left[\frac{R}{R + H} \right] \tag{4-14}$$

and,

$$\rho_m = H \tan \alpha_m \tag{4-15}$$

Hence,

$$\rho_m = H \tan \left[\sin^{-1} \left(\frac{R}{R + H} \right)\right] \tag{4-16}$$

For a height H = 800 km, $\alpha_m = 62.74^\circ$, and

$$\rho_m \text{ (H=800 km)} = 1550 \text{ km} \tag{4-17}$$

Since in the flat E-A system $1^\circ = 100$ km, one has

$$\rho_m' \text{ (H=800 km)} \simeq 15.5^\circ \tag{4-18}$$

As shown in figure 4-1, ρ is the distance between the SSP and the centroid of the area element ΔA under consideration. Therefore, according to the criterion previously discussed for deciding if a given ΔA_i should be considered within the FOV or not, one should compare the corresponding value ρ_i with ρ_m. If $\rho_i \leq \rho_m$, ΔA_i is considered to be within the FOV. Therefore, one can write into the computer program a simple scanning scheme for testing all area elements within the area of interest. Of course, the total of 2592 ΔA's can be scanned each time a particular ΔA is considered for inclusion in the computations, but computer time is saved if one can program the boundaries of an area somewhat larger than the area of interest. This point is illustrated in detail in the following exercise which was actually used to evaluate the validity of the technique being discussed.

Error Free Observations

In this subsection, a spherical radiometer is simulated in a straight line trajectory 800 km above the E-A system. A horizontal flat circular radiometer will be assumed to be coincident with the spherical radiometer at all times and hence the surface area of the E-A system intercepted by both FOV's will be identical. Arbitrarily, six regions and six satellite positions have been selected which are portrayed in figure 4-2. Although a total of fifteen regions are shown in this figure, only six of them are observed at one time or another by the satellites; and hence only the W_e values for these six regions needed to be shown. Nevertheless, the W_e values of eight regions were actually included. The six satellite positions are identified by numbers one through six as the satellites travel from south to north in their common trajectory. The longitude and latitude of the SSP for each observation is shown in parentheses next to the number of the observation. The longitudes and latitudes of the centroids of all area elements can be easily found by referring to the longitudes and latitudes indicated at the margins. For example, the longitudes and latitudes of the centroids of the two area elements positioned north and south of SSP No.4 are as follows.

North: long. 22.5^o, lat. +12.5^o. South: long. 22.5^o, lat. +7.5^o. All the data pertaining to those area elements contained within the eight regions bounded by longitudes 0^o and 40^o, and by latitudes -20^o and 60^o were fed into the computer program generated to test the technique.

In order to illustrate how the results for the situation portrayed in figure 4-2 were obtained, one may consider the area element $\Delta A(12.5,32.5)$, that is the area element whose centroid has longitude 12.5^o and latitude 32.5^o. The perimeter of this area element is shown marked with a broken line in figure 4-2. For purposes of this illustration, satellite position No. 6 which has a SSP at 24^o longitude and 20^o latitude is selected. The first

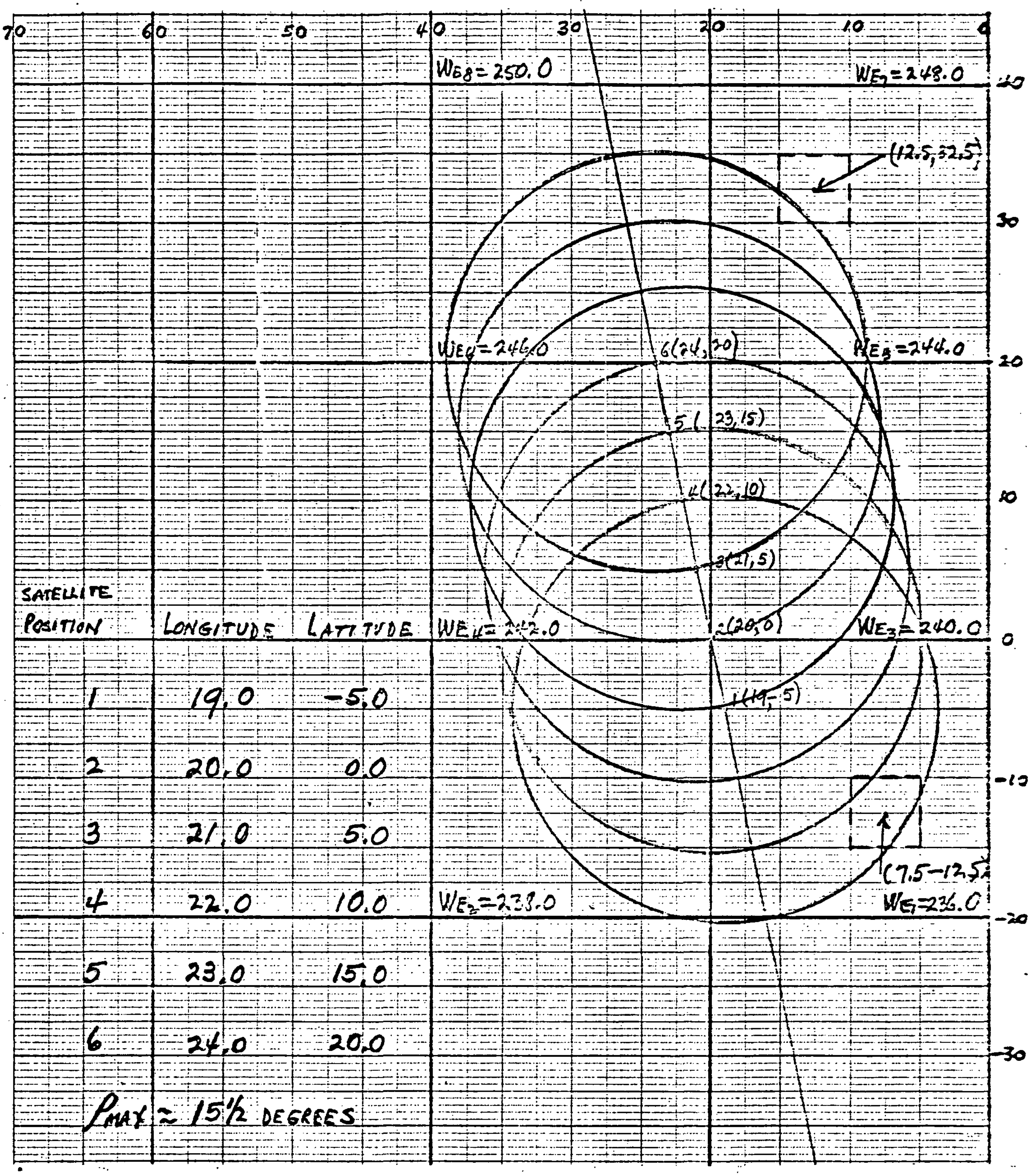

Figure 4-2. Six Satellite FOV's over six regions of the flat E-A system.

step is to compute ρ_6 (12.5,32.5) for this situation and compare it with ρ_{6m} to determine if ΔA (12.5,32.5) is or is not within the FOV of the satellites at position No.6. In this notation the ρ_6 (12.5, 32.5) means the distance (in m) between SSP No.6 and the centroid of ΔA (12.5,32.5); while ρ_{6m} means the radius of the FOV for SSP No.6, which is the maximum value ρ can attain for observation No.6.

As shown in the previous subsection for H = 800 km, $\rho_{6m} = 1.55 \times 10^6$m. Using primes to indicate the distances in <u>degrees</u>, one calculates ρ_6' (12.5,32.5) as follows,

$$\rho' = (\Delta^2_{long} + \Delta^2_{lat})^{\frac{1}{2}} \tag{4-19}$$

where,

$$\Delta^2_{long} = (12.5-24.)^2 = (-11.5)^2 = 132.25$$

$$\Delta^2_{lat} = (32.5-20)^2 = (12.5)^2 = 156.25$$

ρ' = distance from SSP to ΔA in degrees

Then,

$$\rho_6' = (288.5)^{\frac{1}{2}} = 17.0^\circ ; \ \rho_{6m}' = 15.5^\circ \tag{4-20}$$

Hence, $\rho_6' > \rho_{6m}'$, which means that the area element ΔA (12.5, 32.5) is NOT within the FOV of the radiometer at position No.6.

In order to calculate the shape factor and the power increment contributed by an area element (which must lie within the FOV of the satellites) an area element lying inside the FOV of observation No.1 is selected. This element is ΔA (7.5,-12.5) and its boundaries are also marked with a broken line in figure 4-2. Since the whole trajectory is at a height of 800 km, the value of ρ_m for position No.1 is the same as No.6, i.e., $\rho_{1m}' = 15.5^\circ$. The calculation of ρ_1' (7.5,-12.5) is then,

$$\Delta^2_{long} = (7.5 - 19)^2 = 132.25$$

$$\Delta^2_{lat} = (-12.5-(-5))^2 = 56.25 \qquad (4\text{-}21)$$

$$\rho_1' = (188.5)^{1/2} = 13.7^o$$

Thus, $\rho_1' < \rho_{1m}'$ and ΔA (7.5, - 12.5) contributes radiant power to the radiometers of the satellites at position No.1.

In order to simplify the computations of this run, the radiation field was assumed isotropic. This means that in equations (3-18) and (3-19),

$$f(\theta_i) = 1 \quad \text{and} \quad I(f) = 1/2$$

Hence, for a spherical satellite the shape factor for the ith area element in the kth region and within the FOV of the jth observation is

$$F^s_{ijk} = \frac{\Delta A}{\pi} \frac{\cos\theta_{ijk}}{d^2_{ijk}} \qquad (4\text{-}22)$$

From figure 4-1, one obtains for the flat E-A system,

$$\cos\theta_{ijk} = \frac{H}{d_{ijk}}$$

$$d^3_{ijk} = (H^2 + \rho^2_{ijk})^{3/2} \qquad (4\text{-}23)$$

Hence,

$$F^s_{ijk} = \frac{\Delta A}{\pi} \frac{H}{(H^2 + \rho^2_{ijk})^{3/2}}$$

For the case under consideration $\rho_{ijk} = 13.7\text{x}10^5$m, and

$$\Delta A = 2.5\text{x}10^{11}\text{m}^2$$

$$H = 8\text{x}10^5\text{m}$$

Then,

(4-24)

By (3-24) all the shape factors of the area elements within region No.1, and within the FOV of SSP No. 1 are added to yield the first element F_{11}^{s} of the configuration factor matrix. The value of this element was calculated by the computer program TARA 7-15-1, and its value, shown in figure 4-3, is

$$F_{11}^{S} = 0.484847428 \tag{4-25}$$

Then, according to (3-17) for a spherical radiometer with a characteristic area $A_s = \pi a^2 = 1\ m^2$, one can write for the power P_{11}^{s} which region No.1 contributes to observation No.1

$$P_{11}^{S} = F_{11}^{S}\ W_{e1} \tag{4-26}$$

From figure 4-2, $W_{e1} = 236.0\ w/m^2$. Hence,

$$P_{11}^{S} = 114.4239930\ w \tag{4-27}$$

In a similar manner, the radiant power contributed by regions 2,3, and 4 are computed and added to get the total radiant power intercepted by the sphere at position No.1. It is noted that since regions 5 and 6 do not appear within the FOV, their contributions are zero. Then, one writes,

$$P_{1}^{S} = \Delta P_{11} + \Delta P_{12} + \Delta P_{13} + \Delta P_{14} \tag{4-28}$$

$$P_{1}^{S} = F_{11}W_{e1} + F_{12}W_{e2} + F_{13}W_{e3} + F_{14}W_{e4} \tag{4-29}$$

This power was calculated by the computer program and its value, shown in figure 4-3, is

$$P_{1}^{S} = 262.892068914\ w \tag{4-30}$$

An identical procedure would be followed in order to obtain P_1^p for the horizontal flat circular satellite. There is only one difference between the two calculations which can be seen from comparing the expressions for the shape factor of the sphere (3-18) and for the plate (3-19). The latter has an additional factor, namely, cos α_{ijk}. The angle α_{ijk} is the nadir angle of ΔA_{ijk} measured at the satellite, and cos α_{ijk} is used in order to account for the projection of the plate area onto a plane perpendicular to the direction of the radiance N_{ijk} (refer to figure 3-3). In the flat E-A system. $\alpha_{ijk} = \theta_{ijk}$, and hence, $\cos \alpha_{ijk} = \cos \theta_{ijk}$. Thus, from (3-19), the expression for the shape factor for the plate, assuming an isotropic radiation field, is

$$F^p_{ijk} = \frac{\Delta A}{\pi} \frac{\cos^2 \theta_{ijk}}{d^2_{ijk}} \tag{4-31}$$

The values of the variables in this expression are the same as for the sphere. Using the value of cos θ_{ijk} given by (4-23) then, one has,

$$F^p_{ijk} = \frac{\Delta A}{\pi} \frac{H^2}{d^4_{ijk}} \tag{4-32}$$

$$F^p_{ijk} = 0.008 \tag{4-33}$$

In this case this value is one half that of the sphere; however, this ratio varies for different area elements as would be expected. The area element here considered is at the limb where cos α_{ijk} attains its smallest value. For an area element at the nadir position, $\cos \alpha_{ijk} = 1$, and the shape factors for both sphere and plate have identical values.

Again here, adding all the contributions from region No.1 to the plate in position No.1, one obtains the value of F_{11}^p shown in figure 4-4, that is,

$$F_{11}^{p} = 0.378000655 \tag{4-34}$$

Then, again, according to (3-17) for horizontal flat circular radiometer with a characteristic area $A_s = \pi a^2 = 1m^2$ one can write for the power P_{11}^{p} which region No.1 ($W_{e1} = 236.0\ w/m^2$) contributes to observation No.1

$$P_{11}^{p} = 89.20815458\ w \tag{4-35}$$

Again here, the powers contributed by regions 2,3, and 4 are calculated in a similar manner and added in order to obtain the total radiant power intercepted by the plate at position No.1. Since the FOV's of the sphere and plate coincide, regions 5 and 6 must not appear in the FOV of the plate at position No.1 either. The expression for P_1^p equivalent to (4-29) is

$$P_1^p = \sum_{k=1}^{4} F_{1k}\, W_{ek} \tag{4-36}$$

The value of P_1^p calculated by the computer program TARA 7-15-1 is shown in figure 4-4; this value is

$$P_1^p = 190.073940996\ W$$

In the previous paragraphs, it has been shown in detail how to calculate the elements of the configuration factor matrices F and power column matrices {P} for spherical and horizontal flat circular radiometers. The elements of the column matrix $\{W_e\}$ were assumed known in order to simulate and compute the radiant power observed by both satellites. In this manner, the elements of the column matrices {P} for both radiometers were calculated by the computer program. Figures 4-3 and 4-4 show all the elements of the square F matrix and of the two column matrices $\{W_e\}$ and {P}. These figures show the matrix products for the sphere and plate, which can be written symbolically

COFSPH(K,1)	COFSPH(K,2)	COFSPH(K,3)	COFSPH(K,4)	COFSPH(K,5)	COFSPH(K,6)	WE		PSPHER(K)
0.484847428	0.384856899	0.127704158	0.108360067	0.000000000	0.000000000	236.0		262.892068914
0.276829292	0.276829292	0.276829292	0.276829292	0.000000000	0.000000000	238.0		264.648803387
0.108860067	0.127704158	0.384856899	0.484847428	0.000000000	0.000000000	240.0		265.665298558
0.017068977	0.035500329	0.355753027	0.595573384	0.017068977	0.035500329	242.0	=	254.884753820
0.000000000	0.000000000	0.247608706	0.596414856	0.068729515	0.143711947	244.0		255.881625193
0.000000000	0.000000000	0.137012641	0.415871635	0.137012641	0.415871635	246.0		269.259475929

Figure 4-3. Matrix product computed for the sphere.

COFHOR(K,1)	COFHOR(K,2)	COFHOR(K,3)	COFHOR(K,4)	COFHOR(K,5)	COFHOR(K,6)	We		PHORIZ(k)
0.378000855	0.279486438	0.078892673	0.063693275	0.000000000	0.000000000	236.0		190.073940996
0.200205230	0.200205230	0.200205230	0.200205230	0.000000000	0.000000000	238.0		191.396199412
0.063693275	0.078892673	0.279486438	0.378000655	0.000000000	0.000000000	240.0	=	193.360972805
0.008805215	0.018591209	0.251441001	0.471341713	0.008805215	0.018591209	242.0		187.635182979
0.000000000	0.000000000	0.172299495	0.473440034	0.040187252	0.091648780	244.0		188.275656474
0.000000000	0.000000000	0.087326867	0.312709653	0.087326867	0.312709653	246.0		194.868514638

Figure 4-4. Matrix product computed for the plate.

as

$$\{P\} = F\ \{W_e\} \tag{4-37}$$

The first test to which the technique was subjected is the following. Consider the error-free power measurements contained in the column matrices entitled PSPHER(k) and PHORIZ(k) in figures 4-3 and 4-4 respectively. Compute the six values of W_e by operating with the inverses of the configuration factor matrices on the power column matrices as indicated by equation (4-3), that is, by using

$$F^{-1}\{P\} = \{W_e\} \tag{4-38}$$

For the case in which the observations are free of uncertainties, the six values of W_e retrieved should be the same as the six hypothetical values of W_e originally given.

The inverses F^{-1} of the original configuration factor matrices for the sphere and plate are presented in figures 4-5 and 4-6, respectively. It should be noted that the inverses appear in the transposed form which is the order in which the computer, ordinarily, prints out matrices.

The six W_e values obtained when performing the matrix multiplications (for the sphere and the plate) given symbolically by (4-38) were identical to the six original hypothetical W_e values to at least eight decimal places, for both satellites.

The technique was then subjected to the following test. The observations were assumed to include gaussian random uncertaintities. The procedure followed and the results obtained are described in detail in the next subsection.

.126406637E 02	-.136852019E 02	.128539834E 01	-.240860110E 00	-.093927101E 01	.210357918E 01
-.299509655E 02	.403290804E 02	-.137579890E 02	.699220887E 01	-.191839507E 02	.386080888E 01
.322632341E 02	-.463025861E 02	.339027825E 02	-.198634305E 02	.103020142E 03	-.252470553E 02
-.195404147E 02	.286083638E 02	-.286083638E 02	.195404147E 02	-.145767511E 03	.379092813E 02
.491022939E 01	-.718887652E 01	.718887652E 01	-.491022930E 01	.833969093E 02	-.249340703E 02
-.287768318E-01	.421310440E-01	-.421310441E-01	.287768319E-01	-.163760570E 02	.778493063E 01

Figure 4-5. Inverse of original configuration factor matrix, in transposed form, for the sphere.

.131424995E 02	-.146981203E 02	.269545375E 01	-.113983297E 01	.272309581E 01	-.373343722E 00
-.292298882E 02	.422074149E 02	-.157270628E 02	.774441065E 01	-.445058032E 02	.907613661E 01
.323672225E 02	-.498062519E 02	.378035854E 02	-.203645559E 02	.152739147E 03	-.328461452E 02
-.201552571E 02	.315809718E 02	-.315809718E 02	.201552571E 02	-.209818167E 03	.472575341E 02
.499057827E 01	-.781966270E 01	.781966270E 01	-.499057827E 01	.120475873E 03	-.308370566E 02
-.264366054E 00	.414231230E 00	-.414231229E 00	.264386054E 00	-.228348995E 02	.942600877E 01

Figure 4-6. Inverse of the original configuration factor matrix, in transposed form, for the plate.

Perturbed Observations

In order to generate the gaussian random errors needed to perturb the six radiant power measurements, a computer program using two subroutines (RANDU and GAUSS) was generated. The sigma value of the gaussian distribution is $\sigma = 0.5\ W/m^2$. The gaussian errors ε_g were added to the power values originally computed (i.e., the unperturbed powers) in order to obtain the gaussian-perturbed power matrix $\{P_g\}$, that is,

$$\{P\} + \{\varepsilon_g\} = \{P + \varepsilon_g\} = \{P_g\} \tag{4-39}$$

where

P_g = Gaussian perturbed power elements of the new matrix.

The test to which the technique will now be subjected consists in carrying out the multiplication of the configuration factor matrix by the new column power matrix $\{P_g\}$. This multiplication is similar to that in (4-38), except that in the latter, the original power column matrix $\{P\}$ is used instead of $\{P_g\}$. Hence, the old elements of $\{W_e\}$ in (4-38) will be modified by uncertaintities ε_{wg} resulting from the uncertaintities ε_g in the elements of $\{P_g\}$. That is, in matrix form,

$$\{W_e\} + \{\varepsilon_{wg}\} = \{W_e + \varepsilon_{wg}\} = \{W_{eg}\} \tag{4-40}$$

and the matrix product to be calculated can be written as

$$F^{-1}\ \{P_g\} = \{W_{eg}\} \tag{4-41}$$

Where F^{-1} are the inverse matrices given in transposed form for the sphere and the plate in figures (4-5) and (4-6), respectively. The first three results obtained by adding Gaussian random perturbations to the exact power measurements are listed in TABLE 4-1. There are three sets of data in this table. For each set, the gaussian error for each of the regions appears on the first row of the set. The second row contains the uncertaintities ϵ_{wg} in the values of W_e for the six regions, resulting from the perturbations ϵ_g of the power measurements of the spherical radiometer. Similarly, the third row contains the corresponding uncertaintities ϵ_{wg} in the values of W_e for the six regions, for the flat radiometer. Each of the quantities in the last column represents the root-mean-square (rms) values of the six errors shown in the corresponding row. Two important facts are to be noticed from the last column of TABLE 4-1; these are

(a) The plate consistently exhibits a larger error than the sphere.

(b) The results of the matrix inversion are completely unacceptable when the observations include gaussian uncertainties.

At this point, based on the results stated in item (b) above, the applicability of this technique was questioned and therefore, it was decided to investigate the possibility of improving the situation. However, before going into a discussion of how the problem was solved, it will prove helpful to introduce now the results obtained when the observations included systematic uncertainties only, as well as when combinations of systematic and gaussian uncertainties were included.

TABLE 4-2 shows the errors ϵ_{ws} in W_e when systematic errors ϵ_s were added to the power elements of {P}. In this table, two sets of data are presented. Each set has in the first row, the systematic errors ϵ_s for the six regions. The second and third rows, as before, contain the errors ϵ_{ws} in W_e for the sphere and plate, respectively. Systematic errors ϵ_s of equal magnitude and opposite sign produce errors ϵ_{ws} of equal magnitude but opposite sign.

Two conclusions can be made from TABLE 4-2: (a) Systematic errors in

TABLE 4-1. Results obtained from observations having gaussian uncertaintities.

Set No.	Type of Error		Region 1	Region 2	Region 3	Region 4	Region 5	Region 6	rms of All Columns
1	Gaussian,	ε_g*	- 1.1430	- 0.3780	0.0730	0.7630	- 0.3030	0.7480	0.6693
	Sphere,	ε_{wg}*	- 17.1903	21.0556	- 17.8317	12.6009	- 126.0356	36.5961	55.4374
	Plate,	ε_{wg}	- 18.6985	23.9852	- 21.1519	13.9772	- 188.8153	47.0500	81.0685
2	Gaussian,	ε_g	- 0.6290	- 0.0900	0.0220	1.1540	0.0010	0.5750	0.5869
	Sphere,	ε_{wg}	- 27.1069	36.9908	- 31.8555	21.6465	- 169.1907	45.9727	75.6367
	Plate,	ε_{wg}	- 28.3301	41.0255	- 36.1231	22.9781	- 249.4868	58.6197	108.0112
3	Gaussian,	ε_g	- 0.6060	- 0.0060	- 0.5100	- 0.1780	- 0.0350	0.3750	0.3654
	Sphere,	ε_{wg}	- 20.6392	26.8407	- 13.1619	6.9388	- 31.3333	8.6223	20.0993
	Plate,	ε_{wg}	- 20.9824	28.8626	- 15.6265	7.7164	- 54.7122	13.1255	28.1151

* ε_g is in watts

** ε_{wg} is in w/m^2.

TABLE 4-2. Results obtained from observations having systematic errors.

Set No.	Type of Error	Region 1	Region 2	Region 3	Region 4	Region 5	Region 6	rms of All Columns
1	Systematic, ε_s*	- 0.3	- 0.3	- 0.3	- 0.3	- 0.3	- 0.3	0.3
	Sphere, ε_{ws}**	- 0.0882	- 0.5409	0.0094	- 0.4641	0.5549	- 0.4432	0.4123
	Plate, ε_{ws}	- 0.2552	- 0.5636	- 0.1789	- 0.5007	0.3662	- 0.5109	0.4205
2	Systematic, ε_s	0.9	0.9	0.9	0.9	0.9	0.9	0.9
	Sphere, ε_{ws}	0.2646	1.6226	- 0.0283	1.3922	- 1.6648	1.3297	1.2370
	Plate, ε_{ws}	0.7657	1.6907	0.5368	1.5022	- 1.0987	1.5328	1.2614

* ε_s is in watts

** ε_{ws} is in w/m^2

the observations do NOT produce large errors in W_e; and (b) the plate shows larger errors ϵ_{ws} than the sphere.

Combinations of systematic and gaussian errors ϵ_{gs} were included in the power measurements in order to compute the errors ϵ_{wgs} resulting in the W_e values. As expected, these ϵ_{wgs} errors exhibited more sensitivity to the gaussian than to the systematic uncertainties. The results obtained are shown in TABLE 4-3. The results in this table again show that the sphere yields better results than the plate when gaussian random uncertainties are included in the power measurements. So far, however, the two radiometers yield acceptable results only when the errors are systematic.

Thus, as can be seen from the data in TABLES 4-1 and 4-3, the gaussian errors are highly magnified through the matrix multiplication of the inverse of the configuration factor matrix and the perturbed power column matrix. This instability of the inverses of both configuration factor matrices (sphere and plate) was corrected as explained in the following section.

Matrix Stabilization

Prior to describing the scheme developed for stabilizing the two matrices, it is necessary to return to the topic of ill-conditioned perturbed equations in order to introduce the concept of the CONDITION NUMBER of a matrix.

Consider the set of n simultaneous equations represented in (4-1) in matrix form as

$$F\{W_e\} = \{P\} \qquad (4\text{-}42)$$

where

TABLE 4-3. Results obtained from observations having combinations of gaussian and systematic errors.

Set No.	Type of Error		Region 1	Region 2	Region 3	Region 4	Region 5	Region 6	rms of All Columns
1	Gauss,	ε_g*	-1.1430	-0.3780	0.0730	0.7630	-0.3030	0.7480	0.6693
	Systematic,	ε_s*	0.3000	0.3000	0.3000	0.3000	0.3000	0.3000	0.3000
	Total	ε_{gs}*	-0.8430	-0.0780	0.3730	1.0630	-0.0030	1.0480	0.7170
	Sphere	ε_{wgs}**	-17.1021	21.5965	-17.8411	13.0649	-126.5905	37.0394	55.7449
	Plate	ε_{wgs}	-18.4433	24.5488	-20.9730	14.4779	-189.1815	47.5609	81.2855
2	Gauss,	ε_g	-1.1430	-0.3780	0.0730	0.7630	-0.3030	0.7480	0.6693
	Systematic,	ε_s	0.6000	0.6000	0.6000	0.6000	0.6000	0.6000	0.6000
	Total	ε_{gs}	-0.5430	0.2220	0.6730	1.3630	0.2970	1.3480	0.8718
	Sphere	ε_{wgs}	-17.0139	22.1374	-17.8506	13.5290	-127.1454	37.4826	56.0537
	Plate	ε_{wgs}	-18.1881	25.1123	-20.7940	14.9786	-189.5478	48.0718	81.5040
3	Gauss,	ε_g	-1.1430	-0.3780	0.0730	0.7630	-0.3030	0.7480	0.6993
	Systematic	ε_s	0.9000	0.9000	0.9000	0.9000	0.9000	0.9000	0.9000
	Total	ε_{gs}	-0.2430	0.5220	0.9730	1.6630	0.5970	1.6480	1.0890
	Sphere	ε_{wgs}	-16.9257	22.6782	-17.8600	13.9931	-127.7003	37.9258	56.3639
	Total	ε_{wgs}	-17.9328	25.6759	-20.6151	15.4793	-189.9140	48.5828	81.7242

* ε_g, ε_s, and ε_{gs} are in watts

** ε_{wgs} is in w/m^2

F = n by n configuration factor matrix

$\{W_e\}$ = column matrix of n W_e elements

$\{P\}$ = column matrix of n P elements

It is possible that these quantities may include errors resulting from either one, or both, of the following (reference 6).

(a) The data (i.e., the observations $\{P\}$) are inexact.

(b) Rounding errors are generated during computations.

Samples were run with error-free observations and all the W_e values retrieved were accurate to at least eight decimal places. Consequently, one is justified in assuming that computational errors have not caused difficulties, and that only errors of type (a) should be treated in this discussion.

The perturbed equation to be solved is of the form given by (4-4), that is,

$$F\{W_e'\} = \{P + \delta P\} \tag{4-43}$$

where, as indicated in (4-5),

$$\{W_e'\} = \{W_e + \delta W_e\} \tag{4-44}$$

In this expression, the elements of $\{\delta P\}$ are considered to be either gaussian errors ε_g, or systematic errors ε_s, or a combination of both ε_{gs}. It is assumed for purposes of this section that the perturbed equation (4-43) is ill-conditioned, that is, that the inverse matrix F^{-1} is unstable. It can be shown that for ill-conditioning of this type the following relationship exists (reference 6).

$$\text{rel } \{W_e\} = C_2 \cdot \text{rel } \{P\} \tag{4-45}$$

where

$$\mathrm{rel}\{W_e\} = ||\delta W_e|| \,/||W_e|| \qquad \text{(relative error)} \qquad (4\text{-}46)$$

$$\mathrm{rel}\{P\} = ||\delta P|| \,/||P|| \qquad \text{(relative error)} \qquad (4\text{-}47)$$

$$C_2 = ||F|| \cdot ||F^{-1} \qquad \text{(condition number of F)} \qquad (4\text{-}48)$$

The symbol $||\ ||$ denotes the column or row norm of the matrix inside it, as will be explained below.

Condition number. - Even though there are several definitions of the condition number of a matrix (references 6 and 7) only two of them will be introduced in this report.

$$C_1 = \frac{\max|\lambda i|}{\min|\lambda i|} \qquad (4\text{-}49)$$

$$C_2 = ||F|| \cdot ||F^{-1}|| \qquad (4\text{-}50)$$

where

$\max|\lambda i|$ = largest modulus eigenvalue of F

$\min|\lambda i|$ = smallest modulus eigenvalue of F

$||F||$ = Column or row norm of F defined, respectively, as (reference 5)

$$||F||_1 = \max_j \sum_i |F_{ij}| \qquad (4\text{-}51)$$

$$||F||_\infty = \max_i \sum_j |F_{ij}| \qquad (4\text{-}52)$$

For the ill-conditioned situation considered here and represented by the perturbed equation (4-44), it can be seen from (4-46) that ill-conditioning depends on the size of the condition number C_2 and on the relative error rel {P}. Thus, for a given set of power errors {δP}, one would expect that if the original ill-conditioned matrices could somehow be transformed into two well-conditioned matrices, the condition numbers of the latter would be smaller than those of the former.

A computer program was used to obtain the eigenvalues of the two configuration factor matrices and to compute the values of C_1 for both matrices. This program also verified that the eigenvalues computed are correct by making use of the following relations (reference 8)

$$TrF = \sum_i \lambda_i$$

$$|F| = \prod_i \lambda_i$$

where,

TrF = Trace of the matrix F

λ_i = ith eigenvalue of F

$|F|$ = The determinant of F

The values of the condition numbers C_2 for both of the original ill-conditioned matrices were calculated. These values are shown in TABLE 4-4 below.

TABLE 4-4. Condition numbers of the two original matrices.

Type of Sensor	C_1	C_2
Spherical	131.6	693.9
Horizontal flat circular	126.4	684.7

After considerable effort, a scheme was found which rendered both configuration factor matrices well-conditioned and their corresponding values of C_1 and C_2 became much smaller than those shown in TABLE 4-4.

Stabilization procedure.- Essentially, this prodedure consists in translating the smallest elements in the six by six configuration factor matirx. The translation of each element is performed along the row of the element to the position of the diagonal element in that row and it is added to the diagonal element. In this manner, the sum of the elements in the row in question is preserved. This means that the sum of the row elements always adds up to the configuration factor of the total FOV, which is a desirable feature, as will be explained below.

Referring to the two original matrices in figures 4-3 and 4-4, for the sphere and the plate, respectively, one sees that the elements F_{41} and F_{45} are the lowest value elements in both matrices. For the sphere, these two elements have the common value 0.017068977; while for the plate the common value is 0.008805215. In each of the matrices, these two elements were translated and added to the diagonal element F_{44}. For the sphere, the original value of this element was 0.595573384; while for the plate, the value was 0.471341713. The new values of F_{44} for the sphere and plate become, respectively, 0.629711338 and 0.488952143. The physical meaning of this element translation can be best seen when evaluating the error it introduces into the power calculations. The translation of an element means that the element will appear multiplying the W_e value of the column corresponding to the diagonal element rather than the W_e value corresponding to the column where the element originally appeared. As an example of the magnitude of the error introduced, the case of element F_{45} is calculated. $W_{e5} = 244.0\ W/m^2$, and $W_{e4} = 242.0\ W/m^2$. Hence, $\Delta W_e = 242.0-244.0 = -2.0\ W/m^2$, and the power error ΔP introduced is approximately $\Delta P = (-2.0)(0.017)$, or, $\Delta P = -0.034$ W, which is certainly a negligible error. Physically, this error is equivalent to saying that the radiometers at position No.4 looked a little more at the limb of region No.4 and did not see region No.5 at all. Figures 4-7 and 4-8 show the new stabilized matrices for the sphere and plate, respectively. The captions of these figures include the title of the computer program (TARA 7-15-1) which stabilized the matrices and then used them to compute the values of W_e. The stabilization scheme used in this program establishes lower limits for the magnitudes of the matrix elements for each of the two matrices; any element whose value is below the lower limit assigned to its matrix is to be translated as previously described. The limits determined after several trials were 0.032 for the sphere and 0.016 for the plate. A different computer program (TARA 7-15-2) used different lower bounds as the criteria to carry out the translations. These limits were 0.04 for the sphere and 0.02 for the plate. The results obtained with the latter limits were not as good as those obtained with the former.

The errors in W_e obtained with computer program TARA 7-15-1 by first using the two original ill-conditioned matrices and later using the new well-conditioned matrices are presented in TABLE 4-5. Three different data groups are tabulated there. These groups refer to the first set of data appearing in each of TABLES 4-1, 4-2, and 4-3, as is indicated in the first column of TABLE 4-5. These three groups of data correspond to the three types of uncertainties previously introduced, Guassian ε_g, systematic ε_s, and combinations of gaussian and systematic ε_{gs}. The type of inverse matrix F^{-1} used (original or stable), as well as the class of radiometer (sphere or plate), is specified for each row of W_e errors.

The striking differences exhibited by the results compared in TABLE 4-5 is indicative of the effect that stabilization of the configuration factor

COFSPH(K,1)	COFSPH(K,2)	COFSPH(K,3)	COFSPH(K,4)	COFSPH(K,5)	COFSPH(K,6)
0.484847428	0.384856899	0.127704158	0.108360067	0.000000000	0.000000000
0.276829292	0.276829292	0.276829292	0.276829292	0.000000000	0.000000000
0.108360067	0.127704158	0.384856899	0.484847428	0.000000000	0.000000000
0.017068977	0.035500329	0.355753027	0.595573384	0.017068977	0.035500329
0.000000000	0.000000000	0.247608706	0.596414856	0.068729515	0.143711947
0.000000000	0.000000000	0.137012641	0.415871635	0.137012641	0.415871635

Figure 4-7. Stabilized matrix for the sphere. Computer program TARA 7-15-1.

COFHOR(K,1)	COFHOR(K,2)	COFHOR(K,3)	COFHOR(K,4)	COFHOR(K,5)	COFHOR(K,6)
0.378000655	0.279486438	0.078892673	0.063693275	0.000000000	0.000000000
0.200205230	0.200205230	0.200205230	0.200205230	0.000000000	0.000000000
0.063693275	0.078892673	0.279486438	0.378000653	0.000000000	0.000000000
0.000000000	0.018591209	0.251441001	0.488952143	0.000000000	0.018591209
0.000000000	0.000000000	0.172299495	0.473440034	0.040187252	0.091648780
0.000000000	0.000000000	0.087326867	0.312709653	0.087326867	0.312709653

Figure 4-8. Stabilized matrix for the plate. Computer program TARA 7-15-1.

TABLE 4-5. Comparisons of results of original and stabilized matrices for the first set of data shown in TABLES 3-2, 3-3, and 3-4.

Table No.	Type of Error / Type of Matrix		Region 1	Region 2	Region 3	Region 4	Region 5	Region 6	rms of All Columns
3-2	Gauss,	ε_g	- 1.1430	- 0.3780	0.0730	0.7630	- 0.3030	0.7480	0.6693
	Sphere, Original;	ε_{wg}	- 17.1903	21.0556	- 17.8317	12.6009	- 126.0356	36.5961	55.4374
	Sphere, Stable	ε_{wg}	- 4.3780	2.2977	0.9263	- 0.2114	- 30.4585	11.7397	13.4839
	Plate, Original;	ε_{wg}	- 18.6985	23.9852	- 21.1519	13.9772	- 188.8153	47.0500	81.0685
	Plate, Stable;	ε_{wg}	- 6.1246	4.2833	- 1.4500	1.4032	- 57.9194	17.5682	24.9106
3-3	Systematic	ε_s	- 0.3	- 0.3	- 0.3	- 0.3	- 0.3	- 0.3	0.3
	Sphere, Original;	ε_{ws}	- 0.0882	- 0.5409	0.0094	- 0.4641	0.5549	- 0.4432	0.4123
	Sphere, Stable;	ε_{ws}	0.1054	- 0.8243	0.2928	- 0.6576	1.9990	- 0.8188	0.9895
	Plate, Original;	ε_{ws}	- 0.2552	- 0.5636	- 0.1789	- 0.5007	0.3662	- 0.5109	0.4205
	Plate, Stable;	ε_{ws}	- 0.1036	- 0.8011	0.0586	- 0.6523	1.9446	- 0.8664	0.9673
3-4	Gauss	ε_g	- 1.1430	- 0.3780	0.0730	0.7630	- 0.3030	0.7480	0.6693
	Systematic	ε_s	0.3	0.3	0.3	0.3	0.3	0.3	0.3
	Total	ε_{gs}	- 0.8430	- 0.0780	0.3730	1.0630	- 0.0030	1.0480	0.7170
	Sphere, Original;	ε_{wgs}	- 17.1021	- 21.5965	- 17.8411	13.0649	- 126.5905	- 37.0394	55.7449
	Sphere, Stable;	ε_{wgs}	4.1861	2.6868	1.0686	0.1490	- 30.2402	11.9819	13.4409
	Plate, Original;	ε_{wgs}	- 18.4433	24.5488	- 20.9730	14.4779	- 189.1815	- 47.5609	81.2855
	Plate, Stable;	ε_{wgs}	- 5.8109	4.7553	- 1.1795	1.8456	- 57.6776	17.9422	24.8656

matrices has upon the magnitudes of the uncertainties in W_e. For instance the rms values for ε_{wg} (last column, second and fourth rows) were 55.4374 W/m^2 and 81.0685 W/m^2 when W_e was computed with the original matrices for the sphere and plate, respectively. However, when the corresponding stable matrices were used, the values of ε_{wg} were 13.4839 W/m^2 and 24.9106 W/m^2, respectively, as seen from the results in the third and fifth rows of the last column.

The next question that arises is: how do the condition numbers of the stable matrices compare with those of the two original matrices? In TABLE 4-6, the two condition numbers for each of the four matrices are listed.

TABLE 4-6. Condition numbers of the original and stabilized matrices for the sphere and the plate.

TYPE OF SATELLITE	TYPE OF MATRIX	COMPUTER PROGRAM	C_1	C_2
Sphere	Original (Unstable)	TARA 7-15-1	131.6	693.9
Sphere	Stabilized	TARA 7-15-1	59.9	223.4
Sphere	Partially Stable	TARA 7-15-2	71.4	293.6
Plate	Original (Unstable)	TARA 7-15-1	126.4	684.7
Plate	Stabilized	TARA 7-15-1	39.0	218.2
Plate	Partially Stable	TARA 7-15-2	58.6	317.1

In the first and second rows of TABLE 4-6 are presented the condition numbers for the original and stable matrix of the spherical radiometer. The fourth and fifth rows show the corresponding condition numbers for the horizontal flat plate radiometer. These are the four matrices whose results have been discussed up to now and which were used in computer program TARA 7-15-1. However, the third and sixth rows of TABLE 4-6 present the condition numbers of the two matrices obtained by using slightly different lower bounds (0.04 for the sphere and 0.02 for the plate) as was discussed previously. The results obtained by using these matrices did not meet the accuracy requirements and are termed "partially stable" in TABLE 4-6, and were of no further use. These matrices were generated by, and used in, computer program TARA 7-15-2.

Data Quality Prediction

TABLE 4-5 indicates that the errors in W_e for some of the regions are much more significant than those for other regions. For instance, region 5 shows consistently larger errors than the remaining regions for both types of satellites and for all matrices. Hence, even though the results obtained with the stable matrix (third and fifth rows of each data group) are much more acceptable than those obtained with the original matrices (second and fourth rows of each data group), not all of those results obtained with the stable matrices appear equally acceptable. At this point, two important pertinent questions need to be answered.

(a) What are the accuracy requirements for W_e?

(b) Does the form of the <u>original matrix</u> and the magnitude of its elements bear any relation to the errors in W_e obtained for each of the regions? If this relationship exists, can it be linked to the requirements in (a)?

These two questions are thoroughly dealt with in the following two subsections.

<u>Accuracy requirements</u>.- TABLE 4-7 lists the <u>desired</u> and <u>minimum useful</u> tolerances for each of the quantities to be measured for radiation budget determinations. It is seen from this table that the minimum useful

TABLE 4-7. Accuracy Requirements for Radiation Budget Components.

(Recommendations of investigators conference, 1975)

Variable	Accuracy Desired	Accuracy Minimum Useful	Frequency
Solar Intensity	± 1 to 2 W/m^2	± 5 W/m^2	Monthly
Solar Spectrum In Ozone Bands $\Delta\lambda$ = 50A)		± 10%	
Components For Global Net:			
Albedo	± 0.004	± 0.02	Long Term With Monthly Resolution Desired - Seasonal Is Minimum Useful Period
Longwave Exitance	± 1 W/m^2	± 5 W/m^2	
Components For Regional Net:			
Albedo	± 0.02	± 0.08	Monthly For 10° Of Great Circle Latitude And Longitude
Longwave Exitance	± 3 W/m^2	± 15 W/m^2	
Medium Resolution Scanning:			
Albedo	± 0.04		Monthly Averaged Determined From Scanning Data - 10^4 to 10^5 km^2 Spatial Resolution
Longwave Exitance		± 6 W/m^2	

accuracy for monthly averages of the longwave exitance (W_e) of small regions is $\pm$ 15 w/m^2. In the cases presented in TABLE 4-5, however, the values of W_e are instantaneous for all practical purposes since the time interval during which the measurements were taken is of the order of minutes. Hence, the tolerances for these results should be less stringent than those for monthly averages stated above.

It should be pointed out that the accuracy requirements listed in TABLE 4-7 are the results of recommendations made at the Chicago investigators conference of 1975. On the basis of the above tolerance of $\pm$ 15 w/m^2, one can see that from all the W_e values obtained with the two stabilized matrices the only ones which are not acceptable are

(a) Those of region 5 resulting from gaussian, or combinations of gaussian/systematic power errors for the spherical satellite.

(b) Those of regions 5 and 6 resulting also from gaussian or gaussian/systematic power errors for the plate.

The possibility of a connection existing between the structure of the original configuration factor matrix and the stability of its inverse matrix was thoroughly investigated and excellent results were obtained as discussed in the following paragraphs.

Matrix Parameters.- The original configuration factor matrices shown in figures 4-3 and 4-4 for the sphere and plate, respectively, are again introduced here in figures 4-9 and 4-10. However, these latter figures display additional information which will be needed in this discussion. Each of the first six quantities in the last column consist of the sums of the elements in their corresponding rows, and should be approximately equal to the shape factor of the total FOV of the observation corresponding to that row. The seventh quantity in the same column is the sum of the first six quantities. When this sum is divided by six, it yields the average shape factor for the total FOV, which is shown in the last row of the last

	COFSPH(K,1)	COFSPH(K,2)	COFSPH(K,3)	COFSPH(K,4)	COFSPH(K,5)	COFSPH(K,6)	SPHROW(K)
	0.484847428	0.384856899	0.127704158	0.108360067	0.000000000	0.000000000	1.105768551
	0.276829292	0.276829292	0.276829292	0.276829292	0.000000000	0.000000000	1.107317169
	0.108360067	0.127704158	0.384856899	0.484847428	0.000000000	0.000000000	1.105768551
	0.017068977	0.035500329	0.355753027	0.595573384	0.017068977	0.035500329	1.056465024
	0.000000000	0.000000000	0.247608706	0.596414856	0.068729515	0.143711947	1.056465024
	0.000000000	0.000000000	0.137012641	0.415871635	0.137012641	0.415871635	1.105768551
COLUMN SUMS	0.887105765	0.824890678	1.529764721	2.477896661	0.222811133	0.595083912	6.537552870
PERCENTAGES, X	81.416314223	75.706371568	140.397921212	227.415062849	20.449039970	54.615290183	1.089592145

Figure 4-9. Original matrix for the spherical radiometer.

	COFHOR(K,1)	COFHOR(K,2)	COFHOR(K,3)	COFHOR(K,4)	COFHOR(K,5)	COFHOR(K,6)	HORROW(K)
	0.378000655	0.279486438	0.078892673	0.063693275	0.000000000	0.000000000	0.800073041
	0.200205230	0.20020523	0.200205230	0.200205230	0.000000000	0.000000000	0.800820918
	0.063693275	0.078892673	0.279486438	0.378000655	0.000000000	0.000000000	0.800073041
	0.008805215	0.018591209	0.251441001	0.471341713	0.008805215	0.018591209	0.777575561
	0.000000000	0.000000000	0.172299495	0.473440034	0.040187252	0.091648780	0.777575561
	0.000000000	0.000000000	0.087326867	0.312709653	0.087326867	0.312709653	0.800073041
COLUMN SUMS	0.650704375	0.577175549	1.069651704	1.899390561	0.136319334	0.422949643	4.756191165
PERCENTAGES,Y	82.087244037	72.8114824591	34.9380207892	39.610708856	17.196869788	53.355674072	0.792698527

Figure 4-10. Original matrix for the horizontal plate radiometer.

column. This average value is denoted by x for the sphere, and by y for the plate. Each of the quantities in the row entitled "column sums" is the sum of the six quantities above it. The first six elements of the row termed "percentages, x,y" are obtained by dividing each column sum by the average shape factor for the total FOV and multiplying the result by 100.

NOTE: Since the systematic errors do not produce unacceptable results, the following discussion applies only to those cases in which the errors are totally or partially gaussian.

Prediction scheme.- A qualitative prediction classification based solely on the structure of the original matrices was found. It yielded excellent results when compared with the rms's of several W_e errors computed for each of the regions. This rms is based on ten sets of error data; each set has six ε values required to perturb the six power measurements of each observation group.

In order to predict the quality of the data to be retrieved, three distinct data classes were arbitrarily selected. The quality of the W_e values to be retrieved were predicted to be either ACCEPTABLE; POOR, or REJECTABLE, according to the criteria detailed below.

Let SS_j denote the sum of the elements in the jth column of the configuration factor matrix for the sphere, and let SP_j denote the equivalent sum for the plate. It is recalled that x was used to denote the average of the six shape factors for the total FOV of the sphere. Similarly, y was used to denote the equivalent quantity for the plate. Then, using these definitions, the first criterion can be stated as follows:

NOTE: In the following, REJECT means reject the W_e value determined for the jth region from observations by the sphere, in the case of SS_j, or by the plate, in the case of SP_j. Similar meanings should be attached to ACCEPT and POOR.

$$\text{IF } SS_j < 0.2X \qquad \text{REJECT} \tag{4-53}$$

$$\text{IF } SP_j < 0.2Y \qquad \text{REJECT} \tag{4-53'}$$

Otherwise, SS_j and SP_j are subjected to the following tests.

$$\text{IF } SS_j > 1.25X \qquad \text{ACCEPT} \tag{4-54}$$

$$\text{IF } SP_j > 1.25Y \qquad \text{ACCEPT} \tag{4-54'}$$

If this test is not passed, the diagonal element F_{jj} of the j-column of both matrices (F^s_{jj} for the sphere and F^p_{jj} for the plate) are subjected to the following test.

$$\text{IF } F^s_{jj} \leq 0.25\ SS_j \qquad \text{REJECT} \tag{4-55}$$

$$\text{IF } F^p_{jj} \leq 0.25\ SP_j \qquad \text{REJECT} \tag{4-55'}$$

Otherwise, the two sets of quantities are subjected to a final test.

$$\text{IF } F^s_{jj} > 0.6\ SS_j \qquad \text{ACCEPT} \tag{4-56}$$

$$\text{IF } F^p_{jj} > 0.6\ SP_j \qquad \text{ACCEPT} \tag{4-56'}$$

For those cases when F^s_{jj} and F^p_{jj} are between the above two limits, the classification is,

$$\text{IF } 0.25\ SS_j < F^s_{jj} \leq SS_j \qquad \text{POOR} \tag{4-57}$$

$$\text{IF } 0.25\ SP_j < F^p_{jj} \leq 0.6\ SP_j \qquad \text{POOR} \qquad (4\text{-}57')$$

The predictions made on the basis of the above criteria were sufficiently satisfactory to indicate that there is a definite relationship between the quality of the data to be retrieved and the configuration factor matrix of the measurements. This is of great value since a simple analysis of the matrix tells in advance which are the regions whose results should be considered for further processing, as will be discussed in the following subsection.

TABLE 4-8 compares the data quality predictions with the rms's of the errors in W_e for each of the regions. As seen from this table, in every instance the predictions agree with the computed errors in W_e. From TABLE 4-8 the following can also be seen,

(a) In all cases the uncertainties in W_e for the plate are larger than those for the sphere

(b) The only instance in which a REJECTION was predicted was for the plate in region No.5. The W_e errors computed for the plate in this case were, 33.9284 w/m^2 for the gaussian perturbation and 33.8025 w/m^2 for the gaussian/systematic error combination.

It is apparent then that before retrieving the values of W_e from a given set of power measurements, the above scheme will tell which W_e values will be good enough for further processing, such as averaging of data discussed in the next subsection.

Weighted Averages

The n observations required to solve the n simultaneous equations for W_e can be taken within a time interval of any arbitrary length. However, the physical situations represented by the results would be different for

TABLE 4-8. Comparisons of data quality predictions with rms's of computed W_e errors.

Type of Satellite	Type of Power Error (W/m2)		Type of Results	Errors (ϵ_w) in W_e (W/m^2)					
				Region 1	Region 2	Region 3	Region 4	Region 5	Region 6
Sphere	Gaussian,	ϵ_g	Predicted	Poor	Poor	Accept	Accept	Poor	Accept
Sphere	Gaussian,	ϵ_g	Computed	15.2497	19.9081	6.8638	2.9748	17.4476	5.7264
Sphere	Gaussian Plus ($0.9\ W/m^2$) Systematic,	ϵ_{gs}	Computed	15.1991	20.0824	6.8882	3.1020	17.4142	5.8314
Plate	Gaussian,	ϵ_g	Predicted	Poor	Poor	Accept	Accept	Reject	Accept
Plate	Gaussian,	ϵ_g	Computed	15.5824	21.6890	9.0607	3.9728	33.9284	9.0240
Plate	Gaussian Plus ($0.9\ W/m^2$) Systematic,	ϵ_{gs}	Computed	15.4480	21.9173	9.0688	4.2407	33.8025	9.2882

different time interval lengths. At any rate, regardless of the magnitude of the time intervals selected for accomplishing each set of observations, the resulting data can always be averaged out over much longer time periods. For purposes of the present discussion, a set of results will be considered instantaneous if the corresponding set of n observations is taken during a single pass or orbit of the satellite. A total of T sets of data will be considered for averaging in the following discussion.

The following three types of averages were considered,

$$W_{ei} = \frac{\sum_{j=1}^{T} W_{eij}}{T} \tag{4-58}$$

$$W_{ei}^{A} = \frac{\sum_{j=1}^{T} A_{ij} W_{eij}}{\sum_{j=1}^{T} A_{ij}} \tag{4-59}$$

$$W_{ei}^{F} = \frac{\sum_{j=1}^{T} F_{ij} W_{eij}}{\sum_{j=1}^{T} F_{ij}} \tag{4-60}$$

Where,

W_{eij} = the jth determination of the value of W_e for the ith region

A_{ij} = total area seen of the ith region during the jth observation set.

F_{ij} = sum of all the configuration factors of the ith region which entered in the jth set of observations.

T = total number of results, or observations sets, used in the averaging.

W_{ei} = plain average of the value of W_e for the ith region.

W_{ei}^{A} = Weighted average of W_e for the ith region, using the area A_{ij} as weight.

W_{ei}^{F} = Weighted average of W_e for the ith region, using the configuration factor F_{ij} as weight.

The average W_{ei} given by (4-58), assigns equal weights to all the W_e results entering into the averaging process, regardless of the sizes of the segments of the ith region that were within the FOV's of the radiometer, and regardless of the positions that these segments occupied within the radiometer's FOV. Hence, this type of averaging was considered inadequate. The type of average defined by (4-59) takes into account the size of the region segments that entered into the observations; however, two segments of equal area but making different contributions due to their different positions within the FOV are given equal weights, which might be undesirable in some cases. The third type, defined by (4-60) was considered adequate since it does not suffer from either of the shortcomings mentioned above for (4-58) and (4-59).

Thus, weekly or monthly weighted averages (for any time of the day) can be easily obtained from instantaneous results (for the time of day selected) by using the expression (4-60). Although the SWR component is not discussed in detail in this report, a proposed method that is currently under investigation for tackling the problem of reflected SWR will now be discussed.

Proposed Procedure for Computing W_r

When the W_e regions of the E-A system previously defined were considered, it was assumed that the variations of W_e within the region were negligible or barely detectable by the satellite radiation sensing system. Now, one can assume another <u>common characteristic</u> to all area elements within a given region; this is the ALBEDO $A(\zeta_o)$ for a specific solar zenith angle ζ_o. For reasons which will be apparent later, the zenith angle chosen for this common characteristic is $\zeta_o = 0^o$. Before proceeding further, it is advisable to recall the following relationships that were introduced in the section entitled "BASIC IDEAS".

$$W_r(\zeta) = \int_o^{2\pi} d\psi \int_o^{\pi/2} N_r(\theta,\psi,\zeta) \sin\theta \cos\theta \, d\theta \qquad (2\text{-}19)$$

$$A(\zeta) = r(\zeta) = \int_o^{2\pi} d\psi \int_o^{\pi/2} \rho(\theta,\psi,\zeta) \sin\theta \cos\theta \, d\theta \qquad (2\text{-}20)$$

$$A(\zeta) = r(\zeta) = W_r(\zeta)/H(\zeta) \qquad (2\text{-}21)$$

$$\rho(\theta,\psi,\zeta) = N_r(\theta,\psi,\zeta)/H(\zeta) \qquad (2\text{-}22)$$

Then, one can write for those characteristics that have been assumed common to all area elements within a given region the following,

$$W_r(0) = \int_o^{2\pi} d\psi \int_o^{\pi/2} N_r(\theta,\psi,0) \sin\theta \cos\theta \, d\theta = \text{constant} \qquad (4\text{-}61)$$

$$A(0) = r(0) = \int_o^{2\pi} d\psi \int_o^{\pi/2} \rho(\theta,\psi,0) \sin\theta \cos\theta \, d\theta = \text{constant} \qquad (4\text{-}62)$$

However, since at any instant of time the solar zenith angle exhibits spatial variations within any given region; then, $r(\zeta)$, $A(\zeta)$, and $W(\zeta)$ are not necessarily constant within the given region. Then, the problem is, how is one to determine the $W_r(\zeta)$ of a region if the value of $W_r(0)$ for that region is known?

The following is a simple procedure which uses data available from previous satellite observations to provide a quick solution to the above problem.

Figure 5 on page 11 of reference 4 shows several curves which depict relationships between $r(\zeta)$ and $r(0)$ for different types of surface regions of the E-A system. One or several of these curves are selected to represent the reflecting characteristics of the hypothetical regions one has assumed. Consider now the ith area element of the kth region which is within the FOV of the jth observation of a satellite radiometer. This area element is denoted by ΔA_{ijk}, and the radiant power it contributes to the jth measurement is ΔP_{ijk}. The reading from the curve in figure 5 that corresponds to ΔA_{ijk} is denoted by

$$R_{ijk}(\zeta) = r_{ijk}(\zeta)/r_k(0) \tag{4-63}$$

The albedo A and directional reflectance r for ΔA_{ijk} is given by

$$A_{ijk}(\zeta) = r_{ijk}(\zeta) = R_{ijk}(\zeta)\ r_k(0) \tag{4-64}$$

It should be noted that $r_k(o)$ does not have the subscripts i and j since the value $r_k(o) = A_k(o)$ changes <u>only</u> if the region changes.

From (2-21) shown above, one writes

$$W_{rijk}(\zeta) = r_{ijk}(\zeta)\ H_{ijk}(\zeta) = A_{ijk}(\zeta)\ H_{ijk}(\zeta) \tag{4-65}$$

Then, substituting (4-64) into (4-65) one obtains

$$W_{rijk}(\zeta) = R_{ijk}(\zeta)\ r_k(0)\ H_{ijk}(\zeta) \tag{4-66}$$

The expression for the power increment ΔP_{ijk} which the area element ΔA_{ijk} emits in the direction of the satellite is,

$$\Delta P_{ijk} = N_{rijk}(\theta, \psi, \zeta)\ \frac{A_s}{d_{ijk}^2}\ \Delta A_{ijk} \cos \theta_{ijk} \tag{4-67}$$

where,

$N_{rijk}(\theta, \psi, \zeta)$ = Reflection radiance of ΔA_{ijk} in the direction (θ, ψ) due to solar radiation incident from a direction given by the solar zenith angle ζ.

$A_s = \pi a^2$ = Characteristic area of the radiometer, where a is the radius of the radiometer.

d_{ijk} = Distance from ΔA_{ijk} to the radiometer.

θ_{ijk} = Zenith angle of the radiometer as seen from ΔA_{ijk}.

From (2-22) shown above, one writes

$$N_{rijk}(\theta,\psi,\zeta) = H_{ijk}(\zeta)\ \rho_{ijk}\ (\theta,\psi,\zeta) \tag{4-68}$$

Substituting (4-68) into (4-67) and assuming that $A_s = 1m^2$, one obtains

$$\Delta P_{ijk} = H_{ijk}(\zeta)\quad {}_{ijk}(\theta,\psi,\zeta)\ \frac{\Delta A_{ijk}\ \cos\ \theta_{ijk}}{d^2_{ijk}} \tag{4-69}$$

Now, from the corresponding curve in one of the figures B-3, B-4, or B-5 of reference 3, one can read directly (or by using linear extrapolation) the value of the ratio $r(\zeta)/\pi\ \rho(\theta,\ \psi,\ \zeta)$ which will be denoted by R', that is,

$$R'_{ijk}(\theta,\psi,\zeta) = r_{ijk}(\zeta)/\pi\ \rho_{ijk}\ (\theta,\psi,\zeta) \tag{4-70}$$

or,

$$\rho_{ijk}(\theta,\psi,\zeta) = \frac{r_{ijk}(\zeta)}{\pi\ R'_{ijk}(\theta,\psi,\zeta)} \tag{4-71}$$

Substituting (4-71) into (4-69), one obtains

$$\Delta P_{ijk} = H_{ijk}(\zeta)\ \frac{r_{ijk}(\zeta)}{\pi\ R'_{ijk}(\theta,\psi,\zeta)}\ \frac{\Delta A_{ijk}\ \cos\ \theta_{ijk}}{d^2_{ijk}} \tag{4-72}$$

But from (2-21) above, one writes

$$H_{ijk}(\zeta)\ r_{ijk}(\zeta) = W_{rijk}(\zeta) \tag{4-73}$$

Substituting (4-73) into (4-72) one obtains

$$\Delta P_{ijk} = \left(\frac{\Delta A_{ijk}}{\pi}\right)\left[\frac{\cos\ \theta_{ijk}}{R'_{ijk}(\theta,\psi,\zeta)\ d^2_{ijk}}\right] W_{rijk}(\zeta) \tag{4-74}$$

By the definition of the shape, or configuration factor given by (2-2), with $A_s = 1m^2$, one writes

$$\Delta P_{ijk} = F_{ijk}\ W_{rijk}(\zeta) \tag{4-75}$$

Comparison of (4-74) and (4-75) indicates that

$$F_{ijk} = \left(\frac{\Delta A_{ijk}}{\pi}\right)\left[\frac{\cos\ \theta_{ijk}}{R'_{ijk}(\theta,\psi,\zeta)\ d^2_{ijk}}\right] \tag{4-76}$$

In the following discussion, a new type of shape factor will be introduced in order to develop a simple expression for computing the solutions for the reflected SWR component of the energy budget. This new type of shape factor will be termed PSEUDOSHAPE FACTOR.

One can represent $H_{ijk}(\zeta)$ as

$$H_{ijk}(\zeta) = H_k\ (0)\ \cos\ \zeta_{ijk} \tag{4-77}$$

Note that since the value of $H_k(o)$ changes only with changes of region, only the subscript k of the region need be used, just as in the case of $r_k(o)$ and $A_k(o)$.

Substituting (4-77) into (4-65) one obtains

$$W_{rijk}(\zeta) = r_{ijk}(\zeta)\ H_r(0)\ \cos\zeta_{ijk} \tag{4-78}$$

For the case $\zeta=0$, one obtains from this expression,

$$W_{rk}\ (0) = r_k(0)\ H_r(0) \tag{4-79}$$

Again here, only the subscript k is necessary since these three quantities change value only with region changes.

From (4-63) one writes

$$r_{ijk}(\zeta) + R_{ijk}(\zeta)\ r_k(0) \tag{4-80}$$

Substituting (4-80) into (4-78) one obtains

$$W_{rijk}(\zeta) + R_{ijk}(\zeta)\ r_k(0)\ H_k(0)\ \cos\zeta_{ijk} \tag{4-81}$$

And substituting (4-79) into (4-81),

$$W_{rijk}(\zeta) + W_{rk}(0)\ R_{ijk}(\zeta)\ \cos\zeta_{ijk} \tag{4-82}$$

Substitution of (4-82) into (4-74) yields

$$\Delta P_{ijk} = \left(\frac{\Delta A_{ijk}}{\pi}\right)\left[\frac{R_{ijk}(\zeta)\ \cos\theta_{ijk}\ \cos\zeta_{ijk}}{R'_{ijk}\ (\theta,\psi,\zeta)\ d^2_{ijk}}\right]W_{rk}(0) \tag{4-83}$$

From this expression one defines the PSEUDOSHAPE FACTOR F'_{ijk} as

$$F'_{ijk} = \left(\frac{\Delta A_{ijk}}{\pi}\right)\left[\frac{R_{ijk}(\zeta)\ \cos\theta_{ijk}\ \cos\zeta_{ijk}}{R'_{ijk}\ (\theta,\psi,\zeta)\ d^2_{ijk}}\right. \tag{4-84}$$

By comparing the expressions (4-76) for F_{ijk} and (4-84) for F'_{ijk} one sees that these two qualities are related by the following expression.

$$F'_{ijk} = F_{ijk}\, R_{ijk}(\zeta) \cos \zeta_{ijk} \tag{4-85}$$

Let the following quantity be defined,

$$R''_{ijk}(\zeta) = R_{ijk}(\zeta) \cos \zeta_{ijk} \tag{4-86}$$

Then, (4-85) can be rewritten as

$$F'_{ijk} = F_{ijk}\, R''_{ijk}(\zeta) \tag{4-87}$$

For future use, the weighted average value of $R''_{ijk}(\zeta)$ over all those area elements ΔA_{ijk}, of the kth region which appeared at least once within one of the FOV's of the radiometer will now be calculated. Thus, one writes

$$\sum_{i=1}^{I} \sum_{j=1}^{J} F'_{ijk} = \sum_{i,j} F_{ijk}\, R''_{ijk}(\zeta) = R''_{k} \sum_{i,j} F_{ijk} \tag{4-88}$$

where,

- I = total number of area elements of the kth region within the FOV of the jth observation.
- J = the number of observations in which the kth region appears.
- R''_K = weighted average of $R''_{ijk}(\zeta)$ for the kth region.

Thus,

$$R''_{k} = \frac{\sum_{i,j} F'_{ijk}}{\sum_{i,j} F_{ijk}} \tag{4-90}$$

Returning to equation (4-83), one obtains the power P_{jk} contributed by the kth region to the jth observation, by adding up over all the area elements in the kth region. Hence,

$$P_{jk} = \sum_{i=1}^{I} \Delta P_{ijk} \tag{4-91}$$

Then, one obtains the total power detected in the jth observation by adding up all the powers P_{jk} contributed by the K regions, that is

$$P_j = \sum_{k=1}^{K} P_{jk} \tag{4-92}$$

These P_j's are the elements of the power column matrix {P}. In exactly the same manner, one obtains for the configuration factor F_{jk} and the pseudo-configuration factor F'_{jk} that the kth region contributed to the jth observation

$$F_{jk} = \sum_{i=1}^{I} F_{ijk} \tag{4-93}$$

$$F'_{jk} = \sum_{i=1}^{I} F'_{ijk} \tag{4-94}$$

These F'_{jk}'s constitute the elements of the pseudoconfiguration factor matrix F'. Thus, one can write in matrix form,

$$F'\{W_r(O)\} = \{P\} \tag{4-95}$$

where the elements of the column matrix $\{W_r(o)\}$ are the hypothetical values of $W_r(o)$ which were assigned originally to the different regions. Then, by operating on {P} with F'^{-1}, the inverse of F', one obtains back $\{W_r(o)\}$, that is

$$F'^{-1}\{P\} = \{W_r(0)\} \tag{4-96}$$

If this matrix operation retrieves the correct values of $W_r(o)$ that were originally assigned to each of the regions, then one proceeds, as in the one of W_e, to perturb $\{P\}$ with gaussian and systematic errors to test the stability of F'^{-1}.

The next step is to obtain the values of $W_r(\zeta)$ for each of the regions from the corresponding values $W_r(o)$ found through (4-95). This can be done as follows.

Assuming that the kth region appeared in the FOV's of J observations, one can find the total power that this region contributed to the J observations by adding over j the P_{jk} powers given by (4-91), that is,

$$P_k = \sum_{j=1}^{J} P_{jk} \tag{4-97}$$

Similarly, the contribution of all the configuration and pseudoconfiguration factors by the kth region to all the J observations are, from (4-93) and (4-94),

$$F_k = \sum_{j=1}^{J} F_{jk} \tag{4-98}$$

$$F'_k = \sum_{j=1} F'_{jr} \tag{4-99}$$

And from (4-91) and (4-97) is obtained

$$P_k = \sum_{j,i} \Delta P_{ijk} \tag{4-100}$$

By comparing this expression with (4-75), one can write,

$$P_k = \sum_{j,i} F_{ijk} W_{rijk} (\zeta) \tag{4-101}$$

If one defines W_{rk} to be the weighted average of $W_r(\zeta)$ over the kth region for all the J observations, one writes

$$W_{rk} = \frac{\sum_{j,i} F_{ijk} W_{rijk}(\zeta)}{\sum_{j,i} F_{ijk}} \tag{4-102}$$

Then, (4-101) becomes

$$P_k = W_{rk} \sum_{j,i} F_{ijk} \tag{4-103}$$

If now one compares expression (4-100) with equation (4-83) and uses (4-84), one can write,

$$P_k = W_{rk}(0) \sum_{j,i} F'_{ijk} \tag{4-104}$$

Equating (4-103) and (4-104), one obtains

$$W_{rk} = \frac{\sum_{i,j} F'_{ijk}}{\sum_{i,j} F_{ijk}} W_{rk}(0) \tag{4-105}$$

But the ratio on the right is the same as that in (4-90). Hence, one can say that

$$W_{rk} = W_{rk}(0) R''_k \tag{4-106}$$

Where R''_k is the weighted average of $r(\zeta) \cos \zeta / r(o)$ for the kth region for all observations.

Therefore, the essence of the procedure when applied to an actual set of power measurements is as follows. Compute the elements of the configuration and pseudoconfiguration factor matrices. Obtain the inverse matrix F'^{-1} of the pseudoconfiguration factor matrix and operate with it on the column matrix of the power measurements in order to obtain the column matrix $\{W_r(o)\}$. From these elements, the corresponding W_{rk} elements are obtained by application of (4-106).

BEST FIT/INVERSION TECHNIQUE

As was mentioned in the last paragraph of the section entitled "FUNDAMENTALS OF THE TECHNIQUES," the main feature of the Best Fit/Inversion Technique is that the number of observations m is larger than the number of unknowns n. An extension of the method of least squares is used to determine the approximating surface in the n+1 dimensional space. The procedure followed to find the values of W_e is illustrated by a simplified three dimensional case as follows.

Let it be assumed that a satellite has made eighteen observations over two regions. The FOV of each observation is either totally filled by one of the regions, or totally filled by segments of both of the regions. Furthermore, let it be assumed that the W_e values of the two regions, identified as regions 1 and 2, are in the ranges $W_{e1} = 240.0 \pm 5$ w/m and $W_{e2} = 280.0 \pm 5$ w/m^2, as shown in TABLE 5-1. This table shows the configuration factors F_1 and F_2 that regions 1 and 2 contribute to each of the measurements. The hypothetical values of W_{e1} and W_{e2} at the time each observation is taken are also presented in this table, as well as the two partial powers for each of the measurements. These partial powers, for the ith observation, are given by

$$P_i = P_{i,1} + P_{i,2} = W_{ei,1}\, F_{i,1}\, A_s + W_{ei,2} F_{i,2} A_s \qquad (5\text{-}1)$$

Where

$$A_s = 1\text{m}^2 = \text{characteristic area of the radiometer.}$$

Therefore, the eighteen observations can be written as

$$\begin{aligned} W_{e1,1}\, F_{1,1} + W_{e1,2}\, F_{1,2} &= P_1 \\ W_{e2,1}\, F_{2,1} + W_{e2,2}\, F_{2,2} &= P_2 \\ W_{e3,1}\, F_{3,1} + W_{e3,2}\, F_{3,2} &= P_3 \\ W_{e18,1}\, F_{18,1} + W_{e18,2}\, F_{18,2} &= P_{18} \end{aligned} \qquad (5\text{-}2)$$

TABLE 5-1. Hypothetical data about satellite observations of two regions.

Measurement No. Parameter	1	2	3	4	5	6	7	8	9
F_1	0.4	0.5	0.6	0.3	0.7	0.2	0.8	0.1	0.9
F_2	0.6	0.5	0.4	0.7	0.3	0.8	0.2	0.9	0.1
$F = F_1 + F_2$	1.0	1.0	1.0	1.0	1.0	1.0	1.0	1.0	1.0
W_{e1} (w/m^2)	240	241	242	243	239	238	237	244	245
W_{e2} (w/m^2)	280	279	278	277	281	282	283	276	275
P_1 (w)	96.0	120.5	145.2	72.9	167.3	47.6	189.6	24.4	220.5
P_2 (w)	168.0	139.5	115.2	193.9	84.3	225.6	56.6	248.4	27.5
$P = P_1 + P_2$	264.0	260.0	260.4	266.8	251.6	273.2	246.2	272.8	248.0

TABLE 5-1. Hypothetical data about satellite observations of two regions. (Continuation)

Measurement No.

Parameter	10	11	12	13	14	15	16	17	18
F_1	0.0	1.0	0.45	0.55	0.65	0.25	0.35	0.75	0.15
F_2	1.0	0.0	0.55	0.45	0.35	0.75	0.65	0.25	0.85
$F = F_1 + F_2$	1.0	1.0	1.00	1.00	1.00	1.00	1.00	1.00	1.00
W_{e1} (w/m^2)	240	236	235	240	241	242	243	239	238
W_{e2} (w/m^2)	280	284	285	280	281	282	283	279	278
P_1 (w)	0.0	236.0	105.75	132.0	156.65	60.5	85.05	179.25	35.7
P_2 (w)	280.0	0.0	156.75	126.0	98.65	211.5	183.95	69.75	236.3
$P = P_1 + P_2$	280.0	236.0	262.50	258.0	255.30	272.0	269.0	249.0	272.0

The ith equation of this set represents the ith plane in a three-dimensional space whose rectangular coordinates are $F_{i,1}$, $F_{i,2}$, and P_i. The form of the equations indicates that all planes cross the origin of the coordinate system. One assumes further that the data obtained from the observations (i.e., the values of $F_{i,1}$, $F_{i,2}$ and P_i) when plotted in this three dimensional coordinate system become a scatter diagram which can be represented by an APPROXIMATING PLANE (see reference 9) that best fits the data. The equations of this plane will be of the form

$$P = W_{e1} F_1 + W_{e2} F_2 \tag{5-3}$$

and the partial regression coefficients W_{e1} and W_{e2} will be determined by an extension of the method of least squares as follows.

The general form for the equations (5-2) is,

$$P_i = W_{ei,1} F_{i,1} + W_{ei,2} F_{i,2} \tag{5-4}$$

One multiplies this equation through by $F_{i,1}$ to form 18 equations (i=1,...18). These 18 equations are added up to generate the first equation of the set of 2 equations needed to find the 2 unknowns. The second equation required is obtained by multiplying (5-4) by F_{i-2} to form, again, 18 equations which are then added together as before. Thus

$$\sum_{i=1}^{18} P_1 F_{i,1} = W_{e1} \sum_{i=1}^{18} F_{i,1}^2 + W_{e2} \sum_{i=1}^{18} F_{i,1} F_{i,2} \tag{5-5}$$

$$\sum_{i=1}^{18} P_i F_{i,2} = W_{e1} \sum_{i=1}^{18} F_{i,1} F_{i,2} + W_{e2} \sum_{i=1}^{18} F_{i,2}^2 \tag{5-6}$$

In order to simplify the notation, the following quantities are defined.

$$\overline{PF}_1 = \sum_{i=1}^{18} P_i \, F_{i,1}$$

$$\overline{PF}_2 = \sum_{i=1}^{18} P_i \, F_{i,2}$$

$$\overline{F_1^2} = \sum_{i=1}^{18} F_{i,1}^2 \qquad (5\text{-}7)$$

$$\overline{F_2^2} = \sum_{i=1}^{18} F_{i,2}^2$$

$$\overline{F_1 F_2} = \sum_{i=1}^{18} F_{i,1} \, F_{i,2}$$

Using (5-7), equations (5-5) and (5-6) can be written as

$$\overline{PF}_1 = W_{e1} \, \overline{F_1^2} + W_{e2} \, \overline{F_1 F_2} \qquad (5\text{-}8)$$

$$\overline{PF}_2 = W_{e1} \, \overline{F_1 F_2} + W_{e2} \, \overline{F_2^2}$$

As was mentioned before, (5-8) is a set of two equations in the two unknowns W_{e1} and W_{e2} which is required to solve the problem.

A short program was written to solve the set of equations (5-8) by using a matrix inversion subroutine. This program also computes the average values of W_{e1} and W_{e2} in order to compare these results with the coefficient values found by the least squares method. As in previous programs, the original matrix and its inverse were multiplied in order to verify that the result was the identity matrix. The values of W_{e1} and W_{e2} obtained from the eighteen observations are compared in TABLE 5-2 with the average values of the hypothetical distributions of W_{e1} and W_{e2} given in the problem.

TABLE 5-2. Comparison of W_e values computed from error-free data with the averages of the given W_e values.

TYPE OF VALUES	$W_{e1}(w/m^2)$	$W_{e2}(w/m^2)$
By least square method from 18 observations	239.83	279.99
Averages of the given W_e values	240.17	280.17

Two important modifications were introduced in the next application. (a) Six regions, rather than two, were considered and a total of thirty-six observations were made. (b) systematic and gaussian uncertainties were incorporated into the power measurements. It should be pointed out that since the space now considered is 7th dimensional, one can no longer speak of the equation of an approximating plane, but rather of the equation of an approximating surface.

A gaussian random error distribution with a sigma value of 0.5 w/m^2 was used, as well as three values of systematic errors, 0.3 w/m^2, 0.6 w/m^2 and 0.9 w/m^2.

TABLE 5-3 lists five groups of results based on the following types of uncertainties in the observations.

1. No error in the observations.
2. Gaussian errors only included.
3. Systematic (0.3 w/m^2) combined with gaussian errors.
4. Systematic (0.6 w/m^2) combined with gaussian errors.
5. Systematic (0.9 w/m^2) combined with gaussian errors.

The five sets of data in TABLE 5-3 clearly show that the results are not highly sensitive to the gaussian and systematic uncertainties assumed for the power measurement.

It is recalled that the essential difference between this technique and the Instantaneous/Inverse Technique is that in the latter the number of observations m equals the number of unknowns n; while in the former, m is greater than n. However, the basic equations to be used are the same in both cases, namely, equations (3-22) and (3-23) introduced in the section entitled "Mathematical Bases." The configuration factors in these two expressions include the LDF as can be seen from equations (3-18) and (3-19). Furthermore,

TABLE 5-3. Comparison of W_e values computed from data having uncertaintities with the averages of the given W_e values.

TYPE OF DATA	Region 1	Region 2	Region 3	Region 4	Region 5	Region 6
			VALUES OF W_e (w/m^2)			
AVERAGE of Given W_e Values	179.36	200.42	220.44	239.83	259.56	280.44
FROM Error-Free Data	178.09	199.63	221.22	242.15	256.66	280.69
FROM Observations with Gaussian Errors (σ=0.5 w/m^2)	178.38	199.65	221.30	242.06	256.45	280.64
FROM Observations with (0.3 w/m^2) Systematic & Gaussian Errors	178.68	199.95	221.60	242.36	256.75	280.94
FROM Observations with (0.6 w/m^2) Systematic & Gaussian Errors	178.98	200.25	221.90	242.66	257.05	281.24
FROM Observations with (0.9 w/m^2) Systematic & Gaussian Errors	179.28	200.55	222.20	242.96	257.35	281.54

the corresponding expressions for the case of reflected SWR are developed in a manner similar to that employed in the Instantaneous/Inverse Technique.

The results obtained so far by this technique are satisfactory and further work in its application should be pursued.

SPHERICAL EARTH-ATMOSPHERE SYSTEM

Once it had been shown that the techniques for computing W_e yield acceptable results, it was decided to return to the original problem in which a spherical earth-atmosphere system was being considered.

As was mentioned previously, the power integrations are to be accomplished by adding up the power increments reaching the satellite simultaneously from the different area elements whithin the FOV. Hence, the first step was to generate a computer program which would divide the surface area of the earth-atmosphere system into a finite number of area elements of equal area. The data output of this program gives the longitudes and latitudes of the centroid and four boundaries of each of the 2060 area elements. An area element of 250,000 km^2 was found to be adequate. This size corresponds to an area of 500 by 500 km, or approximately 5^o by 5^o of great circle arc. This yielded a total of 2060 area elements, 2058 of which have equal areas ($2.5x10^{11}$ m^2 each). The other two elements are those centered at each of the poles. These have an area of $2.339x10^{11}m^2$ each. This yields a total surface area for the spherical E-A system of $5.149678x10^{14}m^2$. The radius of this system is considered to be $6.40155x10^6$m, which gives a surface area of $5.149679x10^{14}m^2$. Since the radius of a sphere having an area equal to the area of the earth has a radius of $6.37123x10^6$m, it follows that an atmospheric spherical shell of 30.32 km thicness is being included. This is approximately the thickness commonly used (30km) since it was first suggested by Dr. Frederick B. House (reference 10). More than 95% of the total atmosphere is contained within this shell.

The output data of this program is used in the main computer program to calculate the W_e values of a spherical E-A system.

The total shape factors for the sphere and plate were calculated also in this main program by adding up the shape factors of each of the area elements within the FOV of the radiometers. The results are compared below with those obtained analytically.

Radiometer	Configuration factor of the total FOV Numerically	Analytically
Sphere	1.089592145	1.0838471
Plate	0.792698527	0.7901660

These results indicate that it is unnecessary to use area elements of smaller size to perform the numerical integrations.

The results of the investigations presently being performed using a spherical E-A system will be discussed in a subsequent report.

CONCLUSIONS

On the basis of the investigation results reported in this document, the following has been concluded:

1. The Instantaneous/Inversion Technique (including the data quality prediction and matrix stabilization schemes) yields excellent results when applied to radiometer data containing gaussian and systematic errors. The W_e values obtained are acceptable according to the pertinent accuracy requirements displayed in TABLE 4-7.

2. The problem of determining the solar radiation reflected by the E-A system has been cast in a form which requires minimum computer time for calculating W_r and the albedo. It is concluded that this simple formulation represents the optimum method to solve this problem and will soon be implemented.

3. The results obtained from preliminary applications of the Best Fit/Inversion Technique clearly indicate that the errors in W_e calculated by the use of this technique are not highly sensitive to gaussian and/or systematic power uncertaintities. In all cases investigated the W_e values retrieved met the pertinent accuracy requirements in TABLE 4-7.

4. It has been concluded that division of the surface of the E-A system into 2060 area elements of about 2.5×10^5 km^2 each yields accurate results when used in numercial integrations of configuration factors.

REFERENCES

1. House, F.B., Sweet, G.E., et.al., Long-term Zonal Earth Energy Budget Experiment (ZEEBE). A proposal to AAFE. NASA-Langley, 1973.

2. Craig, R.A.: The Upper Atmosphere Meteorology and Physics. Academic Press (New York, N.Y.) 1965.

3. Stevenson, J.A.; and Grafton, J.C.: Radiation Heat Transfer Analysis for Space Vehicles. ASD Technical Report 61-119, Part I. Aeronautical Systems Division, Air Force Systems Command, U.S. Air Force, Wright-Patterson Air Force Base (Ohio), 1961.

4. Raschke, Ehrhard; Vonder Haar, Thomas H.; Pasternak, Musa; and Bandeen, William R.: The Radiation Balance of The Earth-Atmosphere System from Nimbus 3 Radiation Measurements. NASA TN D-7249, 1973.

5. Anon.: Earth Albedo and Emitted Radiation. NASA SP-8067. July 1971.

6. Cohen, A.M.; Cutts, J.F.; Fielder, R.; Jones, D.E.; Ribbans, J.; and Stuart, E.: Numerical Analysis. John Wiley and Sons (New York), 1973.

7. Faddeev D.K.; and Faddeeva, V.N. (Robert C. Williams, translator): Computational Methods of Linear Algebra. W.H. Freedman and Company (San Francisco), 1963.

8. Matthews, Jon; and Walker, R.L.: Mathematical Methods of Physics. W.A. Benjamin, Inc. (New York), 1965.

9. Spiegel, Murray R.: Theory and Problems of Statistics. (Schaum's Outline Series), McGraw-Hill Book Company (New York), 1961.

10. House, Frederick B.: The Radiation Balance of the Earth from a Satellite. Ph.D. Thesis. Department of Meteorology, The University of Wisconsin, 1965.